bioRxiv preprint doi: https://doi.org/10.1101/2023.01.06.522982; this version posted January 6, 2023. The copyright holder for this preprint (which was not certified by peer review) is the author/funder, who has granted bioRxiv a license to display the preprint in perpetuity. It is made available under aCC-BY-ND 4.0 International license.

Somatostatin-expressing neurons in the ventral tegmental area innervate specific forebrain regions and are involved in the stress response

Elina Nagaeva[1*], Annika Schäfer[1], Anni-Maija Linden[1], Lauri V. Elsilä[1], Maria Ryazantseva[2], Juzoh Umemori[3], Ksenia Egorova[1] & Esa R. Korpi[1*]

[1] Department of Pharmacology, Faculty of Medicine, University of Helsinki, Helsinki, Finland

[2] HiLife Neuroscience Center, University of Helsinki, Helsinki, Finland

[3] Gene and Cell technology, A.I. Virtanen Institute for molecular science, University of Eastern Finland, Kuopio, Finland

* corresponding authors

bioRxiv preprint doi: https://doi.org/10.1101/2023.01.06.522982; this version posted January 6, 2023. The copyright holder for this preprint (which was not certified by peer review) is the author/funder, who has granted bioRxiv a license to display the preprint in perpetuity. It is made available under aCC-BY-ND 4.0 International license.

Abstract

Expanding knowledge about the cellular composition of subcortical brain regions demonstrates large heterogeneity and differences from the cortical architecture. Recently, we described three subtypes of somatostatin-expressing (Sst) neurons in the mouse ventral tegmental area (VTA) and showed their local inhibitory action on the neighbouring dopaminergic neurons (Nagaeva et al., 2020). Here, we report that VTA Sst neurons also project far outside the VTA and innervate several forebrain regions that are mainly involved in the regulation of emotional behaviour. When we deleted these VTA Sst neurons several behaviours and drug effects were affected, such as home cage activity, sensitization of locomotor activity to morphine, fear conditioning responses, and reactions to inescapable stress of forced swimming, often in a sex-dependent manner. Interestingly, the majority of these Sst projecting neurons was found to express *Vglut2* and *Th*, but not *Dat*. Together, these data demonstrate that VTA Sst neurons have their selective projection targets, which are distinct from the main targets of VTA dopamine neurons and involved in the regulation of a variety of behaviours mostly associated with the stress response. This, in turn, makes these VTA neurons a meaningful addition to the somatostatinergic system of the brain.

Introduction

The ventral tegmental area (VTA) is a part of the midbrain, from which it sends neuronal projections to many brain structures. It is mainly recognized as the origin of two important dopaminergic pathways: the mesolimbic pathway to the ventral striatum and the mesocortical pathway to the prefrontal cortex, which control motivation and reward-related processes (Björklund and Dunnett, 2007). However, the VTA additionally contains two other major neuronal subtypes: neurons releasing glutamate (Glu) and γ-aminobutyric acid (GABA). In addition to participating in the

bioRxiv preprint doi: https://doi.org/10.1101/2023.01.06.522982; this version posted January 6, 2023. The copyright holder for this preprint (which was not certified by peer review) is the author/funder, who has granted bioRxiv a license to display the preprint in perpetuity. It is made available under aCC-BY-ND 4.0 International license.

local circuits and controlling the neighbouring dopamine (DA) cells (Dobi et al., 2010; Hnasko et al., 2012; Tan et al., 2012), some of these neurons can project outside the VTA and contribute to larger brain circuits. For example, VTA GABA neurons can project to distant brain areas and modulate the activity of those areas separately from DA signalling, by having unique projection targets (Bouarab et al., 2019). It was shown that continuous activation of the inhibitory projections from the VTA to the epithalamic lateral habenula promotes rewarding behaviours independently of the DA neurons (Stamatakis et al., 2013). At the same time, activation of the rostral VTA GABA neurons projecting to the GABA neurons in the dorsal raphe disinhibits serotonin neurons and promotes aversion (Li et al., 2019). On the other hand, many VTA Glu projections travel in parallel with DA pathways (Cai and Tong, 2022), suggesting their sustaining role in DA signalling. It has also been shown that VTA Glu neurons projecting to the nucleus accumbens (NAc) could drive positive reinforcement and promote wakefulness independently from the DA release (Yu et al., 2019; Zell et al., 2020).

Recently, we have described three VTA Sst+ neuron populations with heterogeneous molecular profiles (75% GABA, 18% Glu, and 5% GABA/Glu), location within the VTA and electrophysiological properties (Nagaeva et al., 2020). We also demonstrated that laterally located VTA Sst neurons were able to inhibit neighbouring DA cells via direct GABAergic transmission. In the present study, we demonstrate that there are anterolateral VTA Sst neurons that project to distant forebrain regions and that deletion of these cells affects stress responses, often in a sex-dependent manner. Interestingly, our data suggest that the majority of the projecting Sst neurons is positive for *Vglut2* and *Th*.

bioRxiv preprint doi: https://doi.org/10.1101/2023.01.06.522982; this version posted January 6, 2023. The copyright holder for this preprint (which was not certified by peer review) is the author/funder, who has granted bioRxiv a license to display the preprint in perpetuity. It is made available under aCC-BY-ND 4.0 International license.

Results

VTA Sst neurons innervate several forebrain regions

To find out whether the Sst neurons project outside the VTA, we injected a Cre-dependent anterograde tracer unilaterally into the VTA of Sst-Cre mice and sectioned the whole brain three weeks later to locate the GFP signal of the tracer. We found VTA Sst projections in several forebrain regions. Then, we defined the regions, which consistently had the densest axonal arborisations in all brains studied, using hierarchical clustering and depicted the results as a heatmap (Fig. 1). The VTA Sst neurons were found to have five main consistent projection targets: the ventral pallidum (VP), lateral hypothalamus (LH), the medial part of the central amygdala (CeM), anterolateral division of the bed nucleus of stria terminalis (alBNST), and paraventricular thalamic nucleus (PVT) (Fig. 1 and 2).

Some of the projection targets, such as the LH and VP, are along the way of the medial forebrain bundle (mfb) – the massive neuronal tract connecting the midbrain with the forebrain. To confirm that the VTA Sst axons innervate the targets mentioned and not only pass through, we injected a Cre-dependent retrograde tracer unilaterally into each of these targets (Fig. 3a). Indeed, injections into the CeM, LH, BNST and VP, produced GFP expression in the cell bodies of the VTA Sst neurons located ipsilaterally to the injection site (Fig. S1-S4). However, unilateral injection of the retrotracer into the PVT produced GFP expression bilaterally in the VTA (Fig. 3b). Similarly, we saw traced axons in the left and right parts of the posterior PVT after unilateral VTA injection of the anterograde tracer (Fig. 2b). This might suggest that either individual VTA Sst neurons can send collaterals to the right and left parts of the PVT, or different Sst neurons from the same VTA side innervated the PVT bilaterally. Another explanation may lie in the non-bilateral

bioRxiv preprint doi: https://doi.org/10.1101/2023.01.06.522982; this version posted January 6, 2023. The copyright holder for this preprint (which was not certified by peer review) is the author/funder, who has granted bioRxiv a license to display the preprint in perpetuity. It is made available under aCC-BY-ND 4.0 International license.

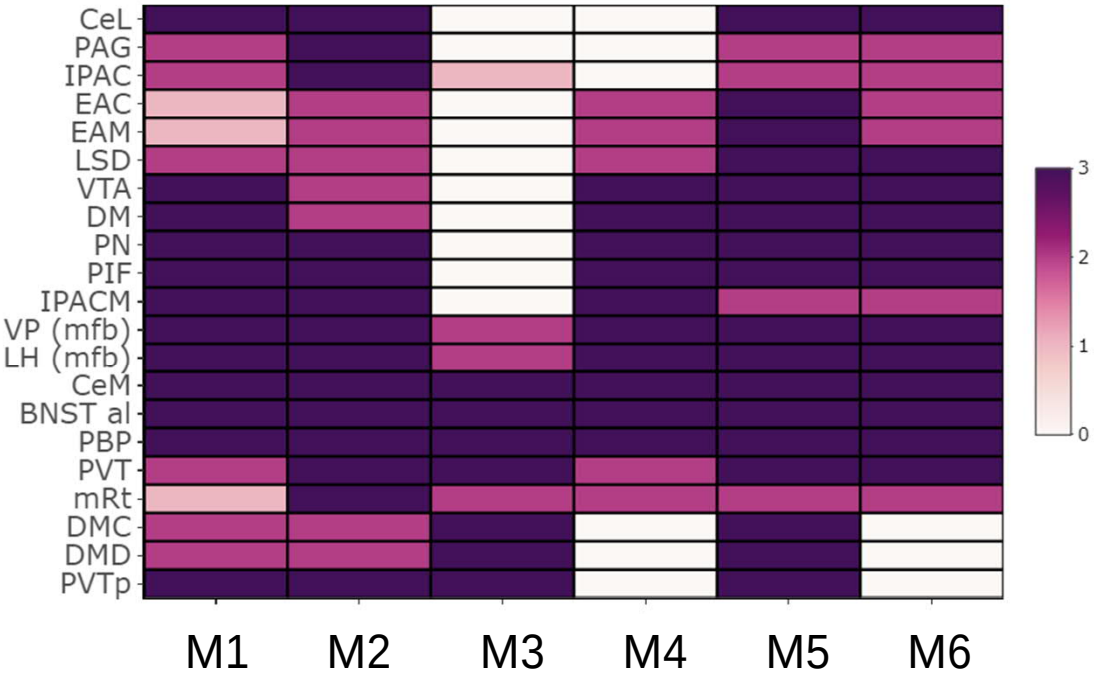

Figure 1. Heatmap of the VTA Sst neuron projections. The brain regions with the densest innervation are shown. Colours indicate the density of the fluorescent axons in the projection site from 0 (no projections) to 3 (highest density). The Y-axis depicts the names of the regions, X-axis shows the mouse number: M1 – mouse 1 and etc.

BNST al – bed nucleus of the stria terminalis, antero-lateral part; *CeL* – central amygdala, lateral part; *CeM* – central amygdala, medial part; *DM* – dorsomedial hypothalamic nucleus; *DMC* – DM, compact part; *DMD* – DM, dorsal part; *EAC* – extended amygdala, central part; *EAM* – extended amygdala, medial part; *IPAC* – interstitial nucleus of the posterior limb of the anterior commissure; *IPACM* – IPAC, medial part; *LH* – lateral hypothalamus; *LSD* –lateral septal nucleus, dorsal part; *mRT* – mesencephalic reticular formation; *PAG* – periaqueductal gray; *PBP* – parabrachial pigmented nucleus of the VTA; *PIF* – parainterfascicular nucleus of the VTA; *PN* – paranigral nucleus of VTA; *PVT* – paraventricular nucleus of the thalamus; *PVTp* – PVT, posterior part; *VP (mfb)* – ventral pallidum (medial forebrain bundle); *VTA* – ventral tegmental area.

bioRxiv preprint doi: https://doi.org/10.1101/2023.01.06.522982; this version posted January 6, 2023. The copyright holder for this preprint (which was not certified by peer review) is the author/funder, who has granted bioRxiv a license to display the preprint in perpetuity. It is made available under aCC-BY-ND 4.0 International license.

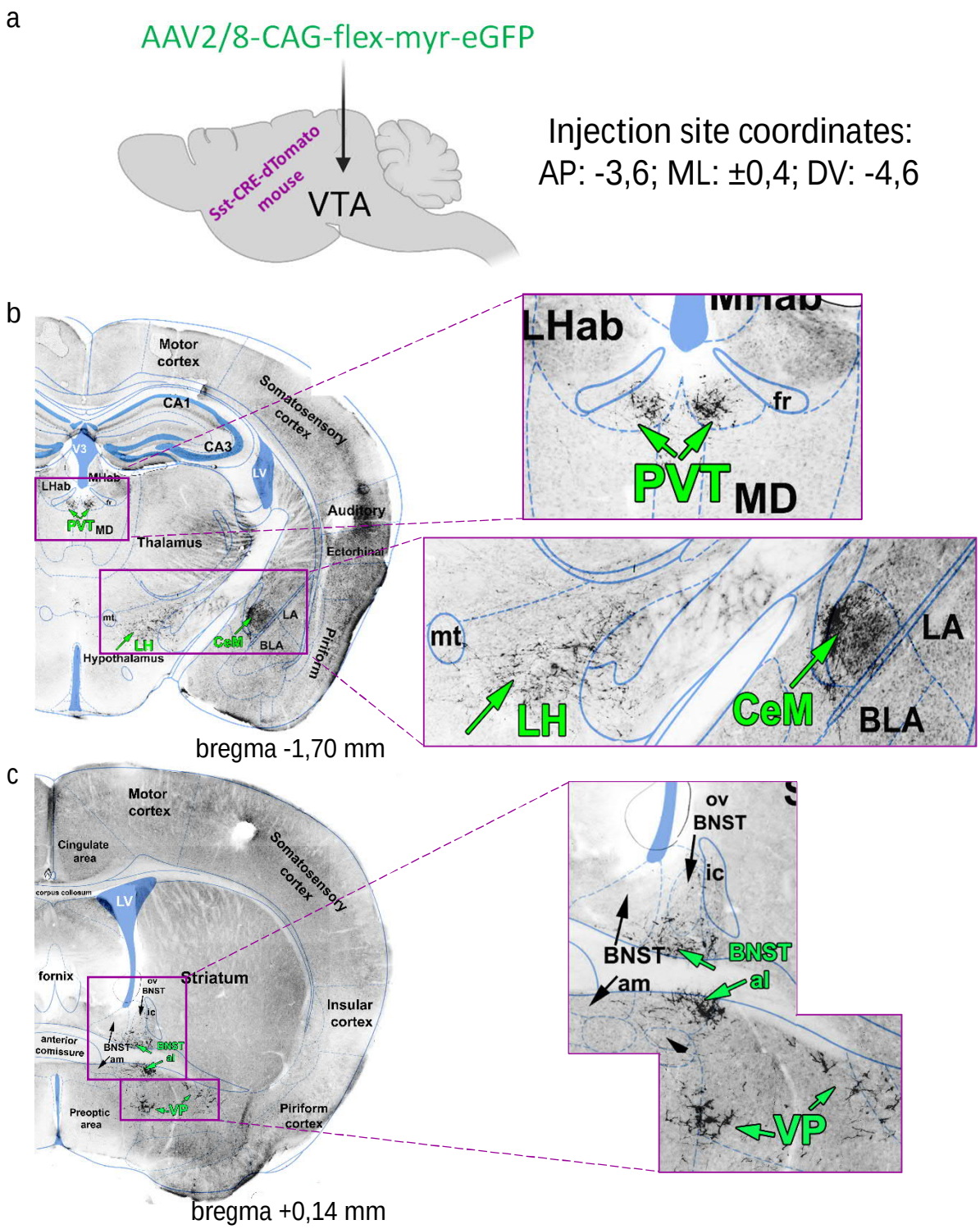

Figure 2. Anterograde tracing of the VTA Sst neurons. a. Sst-tdTomato mice received a unilateral intra-VTA injection of a Cre-dependent AAV tracer. The scheme shows the name of the viral tracer and injection coordinates. b. Examples of the VTA Sst+ projections found in the PVT, LH and CeM at the bregma level -1.70 mm. c. Examples of the VTA Sst+ projections found in the alBNST and VP at the bregma level +0.14 mm. b-c images are the black and white variants of the fluorescent GFP+ images of the coronal mouse brain sections.

bioRxiv preprint doi: https://doi.org/10.1101/2023.01.06.522982; this version posted January 6, 2023. The copyright holder for this preprint (which was not certified by peer review) is the author/funder, who has granted bioRxiv a license to display the preprint in perpetuity. It is made available under aCC-BY-ND 4.0 International license.

anatomy of the PVT, which is the member of the midline thalamic nuclei family (Kirouac, 2015).

The majority of VTA Sst projecting neurons have electrophysiological ADP subtype and express *Th* and *Vglut2*

Retrograde tracing experiments also showed the location specificity of the VTA Sst projecting neurons in the VTA. Most (64/88 analyzed) of the backtraced neurons were found in the anterolateral part of the VTA at the bregma levels between -2.9 and -3.3 mm, with more than half of the cells found at the bregma levels -3.08 and -3.16 mm (Fig. 3c, 4b). We previously demonstrated that different electrophysiological subtypes of the VTA Sst neurons have distinct locations, assigning anterolateral VTA neurons to either afterdepolarizing (ADP) or high-frequency firing (HFF) subtypes (Nagaeva et al., 2020). Therefore, we took an effort to define the electrophysiological subtype of the projecting neurons. To do that, we repeated the same procedure that was used for the backtracing experiments and performed patch-clamp recordings on GFP-positive VTA neurons. We also took advantage of the patch-clamp method to be combined with single-cell mRNA extraction (Cadwell et al., 2017; Fuzik et al., 2016; Sucher and Deitcher, 1995) and used the collected cell contents for further PCR analysis of the expression of main neurotransmitter markers.

For the classification of electrophysiological subtypes of projecting Sst cells, we applied automatic firing pattern analysis (Nagaeva et al., 2021) and clustering algorithm (Nagaeva et al., 2020). We used our previously published electrophysiological dataset containing the firing patterns of 389 VTA Sst neurons as the reference dataset in the clustering procedure (for the full description of the method and reference dataset, see Nagaeva et al., 2020). The majority (67%) of the backtraced neurons were assigned to the ADP cluster (Fig. S5b). Indeed, these neurons showed adapting firing rates at the saturated level of excitation, sag

bioRxiv preprint doi: https://doi.org/10.1101/2023.01.06.522982; this version posted January 6, 2023. The copyright holder for this preprint (which was not certified by peer review) is the author/funder, who has granted bioRxiv a license to display the preprint in perpetuity. It is made available under aCC-BY-ND 4.0 International license.

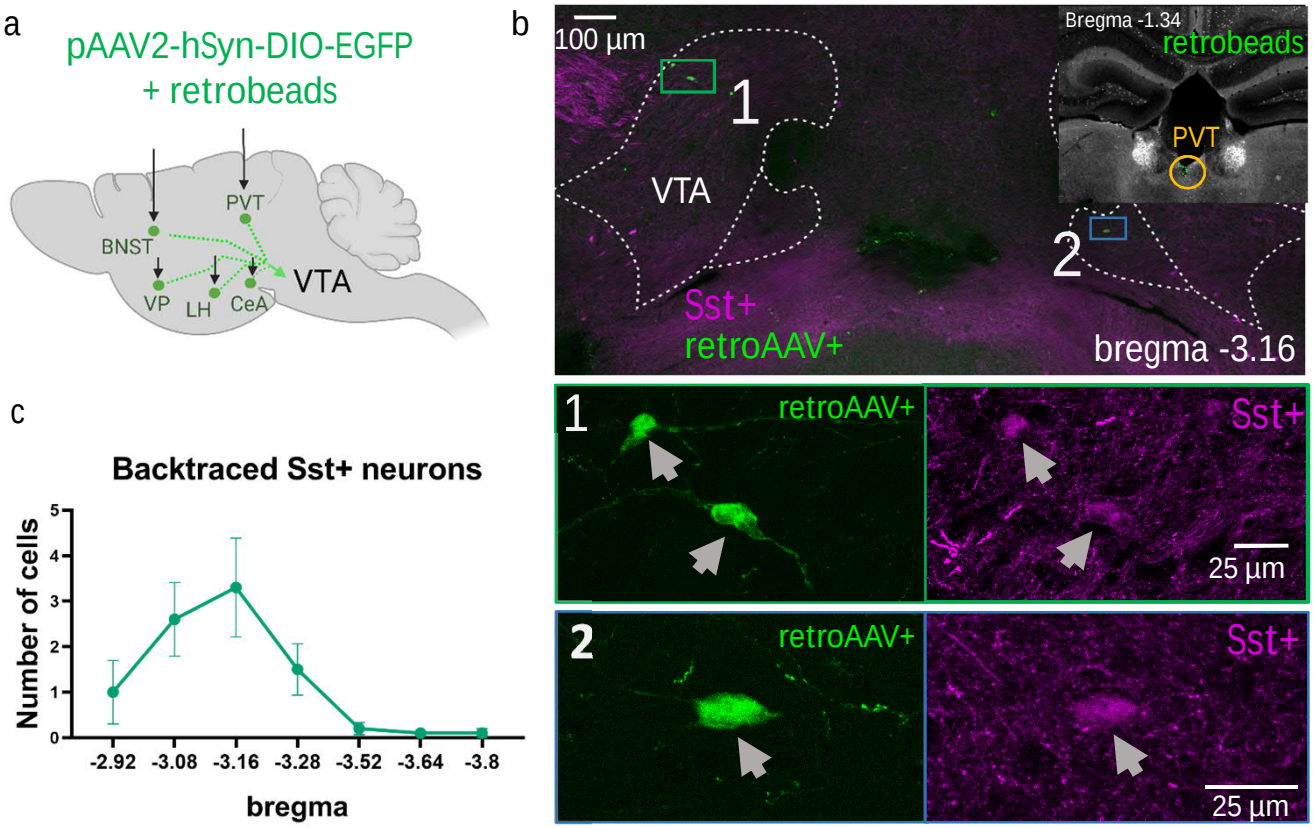

Figure 3. Retrograde tracing of the VTA projecting Sst neurons. a. Sst-tdTomato mice each received a unilateral injection of the mixture of the Cre-dependent retro-AAV virus and retrobeads in one of the five found VTA Sst projection targets (Fig.2). b. Examples of the backtraced neurons in the VTA at the bregma level -3.16 mm. The right upper corner shows retrobeads (green dots) in the injection site within the PVT (yellow circle). The green rectangle shows ipsilaterally traced neurons (1) and the blue rectangle shows a contralaterally traced neuron (2). Lower panels 1 and 2 are the magnified images of the green and blue rectangles. c. The graph shows the distribution of the backtraced VTA neurons at different bregma levels. The number of the backtraced Sst+ neurons from 5 different targets (LH, CeM, PVT, BNST and VP) were combined and are shown as average ± S.E.M. (n=10 mice).

bioRxiv preprint doi: https://doi.org/10.1101/2023.01.06.522982; this version posted January 6, 2023. The copyright holder for this preprint (which was not certified by peer review) is the author/funder, who has granted bioRxiv a license to display the preprint in perpetuity. It is made available under aCC-BY-ND 4.0 International license.

depolarization and small afterdepolarization in the first rheobase action potential (Fig. 4a), mimicking the ADP Sst subtype. Antero-lateral location of the recorded neurons (Fig. 4b) also supported their affiliation with the ADP subtype.

qPCR analysis of the recorded Sst neurons suggested that 78% (18/23 analyzed) of the neurons expressed tyrosine hydroxylase (*Th)* mRNA and 72% (16/23 analyzed) *Vglut2* mRNA with 13/23 cells having both *Th* and *Vglut2* transcripts (Fig. 4c). To address the question of the possible contamination and to have a positive control for the DAergic nature, we also analyzed four DA neurons from the VTA of Th-EGFP mice using the same procedure (DA1-DA4 in the Fig. 4c). These control DA cells expressed a combination of all classical dopaminergic markers, including *Th*, DOPA decarboxylase (*Ddc*) and dopamine reuptake transporter (*Dat*). None of the backtraced VTA Sst+ neurons was found to express the same full set of DA markers (Fig. 4c). Importantly, the control DA neurons did not express any other tested genes, suggesting a low level of contamination from surrounding cells during the cell collecting procedure. Interestingly, we were able to detect *Sst* mRNA in very few of the recorded neurons, although in our mouse model, GFP could be expressed in these neurons only via a Cre-dependent mechanism under the Sst promotor. This fact might be explained by the low level of Sst mRNA expression in Sst-Cre homozygous mice (Viollet et al., 2017). Only 2 out of 23 analyzed Sst projecting neurons showed expression of a combination of the two major GABAergic markers *Vgat* and *Gad1*. We did not observe any specificity in expression profiles depending on the projection target.

Behavioural consequences of the deletion of VTA Sst neurons

We used “the loss of function” approach to elucidate the behavioural impact of the VTA Sst neurons and selectively deleted them by injecting a Cre-dependent caspase-expressing virus bilaterally into the VTA area of adult Sst-Cre-tdTomato

bioRxiv preprint doi: https://doi.org/10.1101/2023.01.06.522982; this version posted January 6, 2023. The copyright holder for this preprint (which was not certified by peer review) is the author/funder, who has granted bioRxiv a license to display the preprint in perpetuity. It is made available under aCC-BY-ND 4.0 International license.

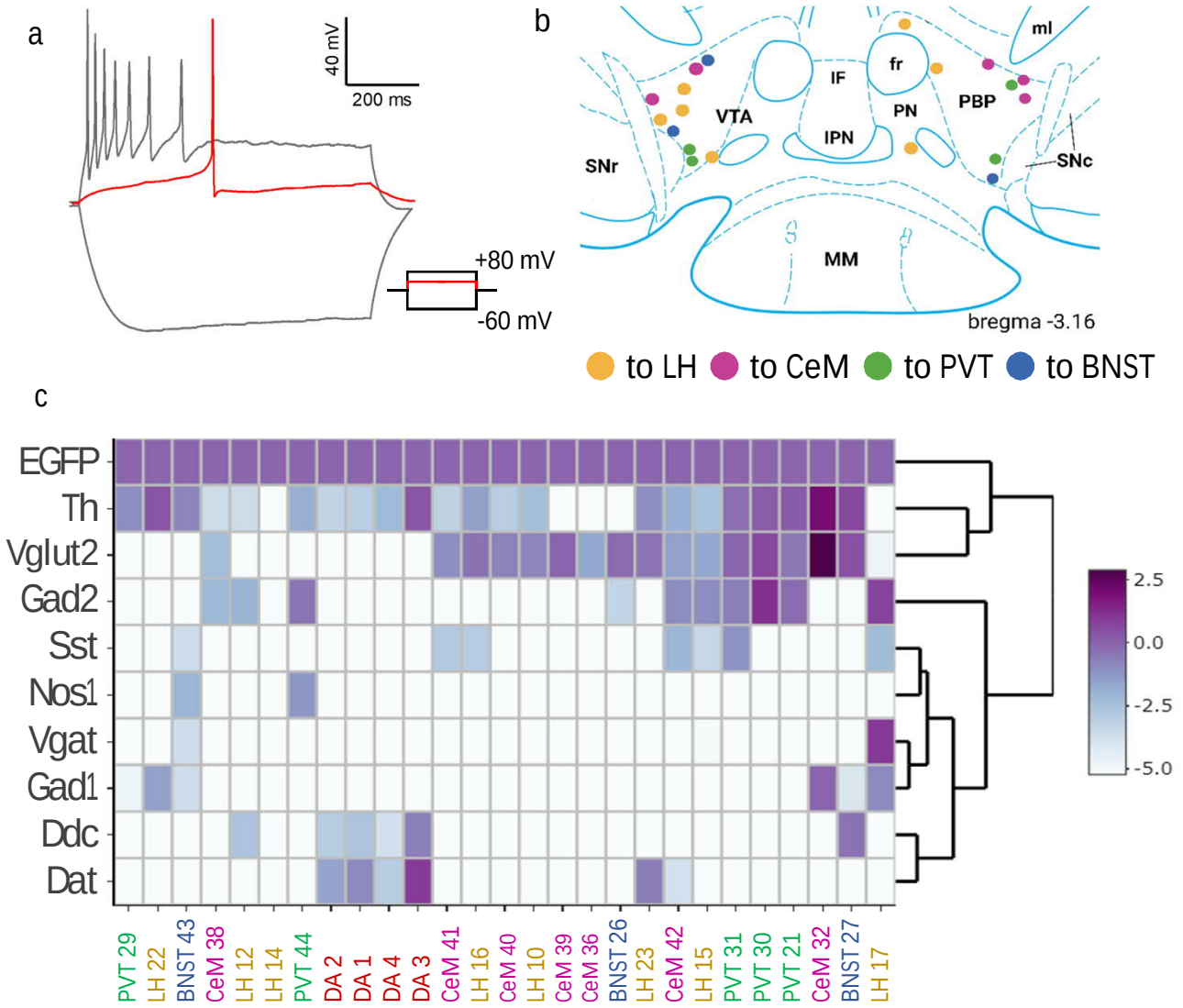

Figure 4. Electrophysiological and expression profiles of the VTA neurons projecting to the forebrain. a. A representative trace of the response of a VTA Sst projecting neuron to injected 800-ms current steps of -60, +8 (red line) and +80 mV. Adapting firing pattern at -80 mV and no delay before the firing resemble features of the ADP Sst subtype (see Nagaeva et al., 2020). b. Locations of the recorded VTA Sst neurons at the bregma level -3.16 mm. Their projection sites are colour-coded. c. The heatmap shows single-cell qPCR results for the main neurotransmitter markers of the backtraced VTA neurons. *EGFP* expression was used as a reference gene and has an expression value of 1. The majority of VTA Sst projecting neurons show expression of *Th* or *Vglut2*, or both, and lack of *Vgat* and *Dat*. Hierarchical clustering analysis did not indicate any neurotransmitter specificity depending on the projecting target. Cell names and colour codes on the X-axis represent the projection site of the cells. DA 1-4 are “control” dopamine cells from Th-EGFP mice and showed detectable expression levels of *Th*, *Dat* and *EGFP*.

bioRxiv preprint doi: https://doi.org/10.1101/2023.01.06.522982; this version posted January 6, 2023. The copyright holder for this preprint (which was not certified by peer review) is the author/funder, who has granted bioRxiv a license to display the preprint in perpetuity. It is made available under aCC-BY-ND 4.0 International license.

mice. After activation, this virus started the programmed cell death and eliminated Sst neurons exclusively in the injected region (Yu et al., 2019), resulting in "VTA^{Sst-} mice". To visualize successful deletion, the GFP-expressing Cre-dependent virus was injected either together with the caspase virus or alone into the control group (Fig. S6). We aimed to delete neurons preferably in the anterolateral VTA, where most of the projecting Sst neurons were found (see Fig. 3c).

For the proper planning of the behavioural experiments, we considered the previously established interneuronal function of ADP Sst neurons (Nagaeva et al., 2020) and the physiological function of their projection targets. Since, on one hand, VTA Sst ADP neurons can inhibit locally neighbouring DA neurons, we used several reward and motivation-related tasks to find out how the impairment of the local inhibitory circuitry affects these processes (Corre et al., 2018; Van Zessen et al., 2012). On the other hand, since they project to forebrain targets such as the PVT, CeM, LH, VP and BNST implicated in the processing of the aversive stimuli and defensive behaviours (Gao et al., 2020; Gomes-de-Souza et al., 2021; Keifer et al., 2015; Lebow and Chen, 2016), we used stress-, anxiety- and fear-related behavioural tests. It was also important to find out whether there were any sex differences in the affected behaviours, as some of the VTA Sst projection targets, such as the PVT, BNST and LH, are known to be sexually dimorphic structures (Kim et al., 2017; López-Ferreras et al., 2017; Uchida et al., 2019).

Increase in home-cage activity of VTA^{Sst-} female mice

Table 1 contains information of the behavioural experiments, the numbers of animals tested in the control and VTA^{Sst-} groups, and whether or not we found statistically significant changes in behaviour. Of the 18 tests performed, only 5 showed noticeable differences between the VTA^{Sst-} and control groups. Interestingly, half of the differences were sex-specific. The VTA^{Sst-} females were more active in

bioRxiv preprint doi: https://doi.org/10.1101/2023.01.06.522982; this version posted January 6, 2023. The copyright holder for this preprint (which was not certified by peer review) is the author/funder, who has granted bioRxiv a license to display the preprint in perpetuity. It is made available under aCC-BY-ND 4.0 International license.

Table 1

Behavioural tests for VTA^{Sst+} and VTA^{Sst-} mice

Name of the test	Environment	group size				Affected?	Statistical significance in
		♂ control	♂ caspase	♁ control	♁ caspase		
Running wheel	home cage	9	6	8	5	No	-
Open field	open arena	10	9	11	8	No	-
Light-dark box	test system	10	9	11	8	No	-
Elevated plus maze	test system	10	9	11	8	No	-
Novely suppresed feeding	open arena	10	9	11	8	No*	tendency to sex-treatment interaction; caspase males start eating faster than controls, and caspase females later than controls
Sucrose preference	home cage	10	9	11	7	No	
Morphine-induced locomotor sensitization	open arena	10	7	11	8	Yes	expression of morphine sensitization, caspase mice display stronger moprhine-induced locomotor sensitzation
Forced swim test	test system	10	9	11	8	Yes	caspase animals struggle longer than controls
Saccharine preference	Intellicage	7	7	7	5	No	
Home cage activity in group	Intellicage	7	7	7	5	Yes	females are more active in nose-poking to water-containing doors than males; caspase females are more active than control females.
Delay discounting	Intellicage	7	7	7	5	No*	Strong sex interaction; females are ready to wait longer for the saccharine than males.
Reward-related learning	Intellicage	7	7	7	5	No	-
Reward-related unlearning	Intellicage	7	7	7	5	No	-
Reward-related unlearning with punishment	Intellicage	7	7	7	5	No	-
Reward-related re-learning	Intellicage	7	7	7	5	No	-
Fear conditionning (FC)	test system	6	7	5	5	Yes	sex-treatment interaction; caspase males freeze less and caspase females freeze more than controls
FC context test	test system	6	7	5	5	Yes	sex-treatment interaction; caspase males freeze less and caspase females freeze more than controls
FC cue test	test system	6	7	5	5	No	-

bioRxiv preprint doi: https://doi.org/10.1101/2023.01.06.522982; this version posted January 6, 2023. The copyright holder for this preprint (which was not certified by peer review) is the author/funder, who has granted bioRxiv a license to display the preprint in perpetuity. It is made available under aCC-BY-ND 4.0 International license.

nose-poking to the water-containing doors in the corners during the first 14 h in the Intellicage environment than the control females (Fig. 5a). Their activity remained upregulated after adaptation to the Intellicage (during 39-62 h after start), suggesting that differences were not due to exploration of the novel environment. It is important to note that the number of licks to water bottle tips behind the doors was similar in all mouse groups, indicating no increase in water consumption in the VTA^{Sst-} females, or in the females overall compared to males (data not shown). Similarly, we did not see any differences in the open-field and anxiety tests between the control and VTA^{Sst-} mice (Fig. S8, Table S3), suggesting that deletion of the VTA Sst neurons influenced exclusively the home-cage activity in females and not the explorative activity or the level of anxiety. There were no changes in these tests between the control and VTA^{Sst-} male mice (Fig. 5b, Fig. S8).

Fear conditioning is affected differently in VTA^{Sst-} males and females

Considering that VTA Sst neurons mostly project to the brain areas which control response and memory formation to aversive events (Concetti et al., 2020; Goode and Maren, 2017; Keifer et al., 2015; Penzo et al., 2015), we further assessed possible changes in threat processing. We used a Pavlovian fear conditioning paradigm (Maren, 2001), followed by contextual and cue-induced retrieval tests to assess differences in acquisition (acute response) and fear memory formation/expression. During the acquisition, mice were presented with three consecutive 30-s cue sounds (CS) co-terminated with 2-s foot shocks (0.6 mA) and separated with short breaks (Fig. 6a). Repeated measures two-way analysis of variance (ANOVA) for the percent freezing and number of the freezing episodes detected a significant sex*treatment interaction (Table S2, p=0.004 and p=0.035, respectively), indicating that the deletion of VTA Sst neurons influenced reaction to the aversive foot-shock stimuli in a sex-dependent manner. Deeper analysis of the data showed that this difference came exclusively from the time points between the

bioRxiv preprint doi: https://doi.org/10.1101/2023.01.06.522982; this version posted January 6, 2023. The copyright holder for this preprint (which was not certified by peer review) is the author/funder, who has granted bioRxiv a license to display the preprint in perpetuity. It is made available under aCC-BY-ND 4.0 International license.

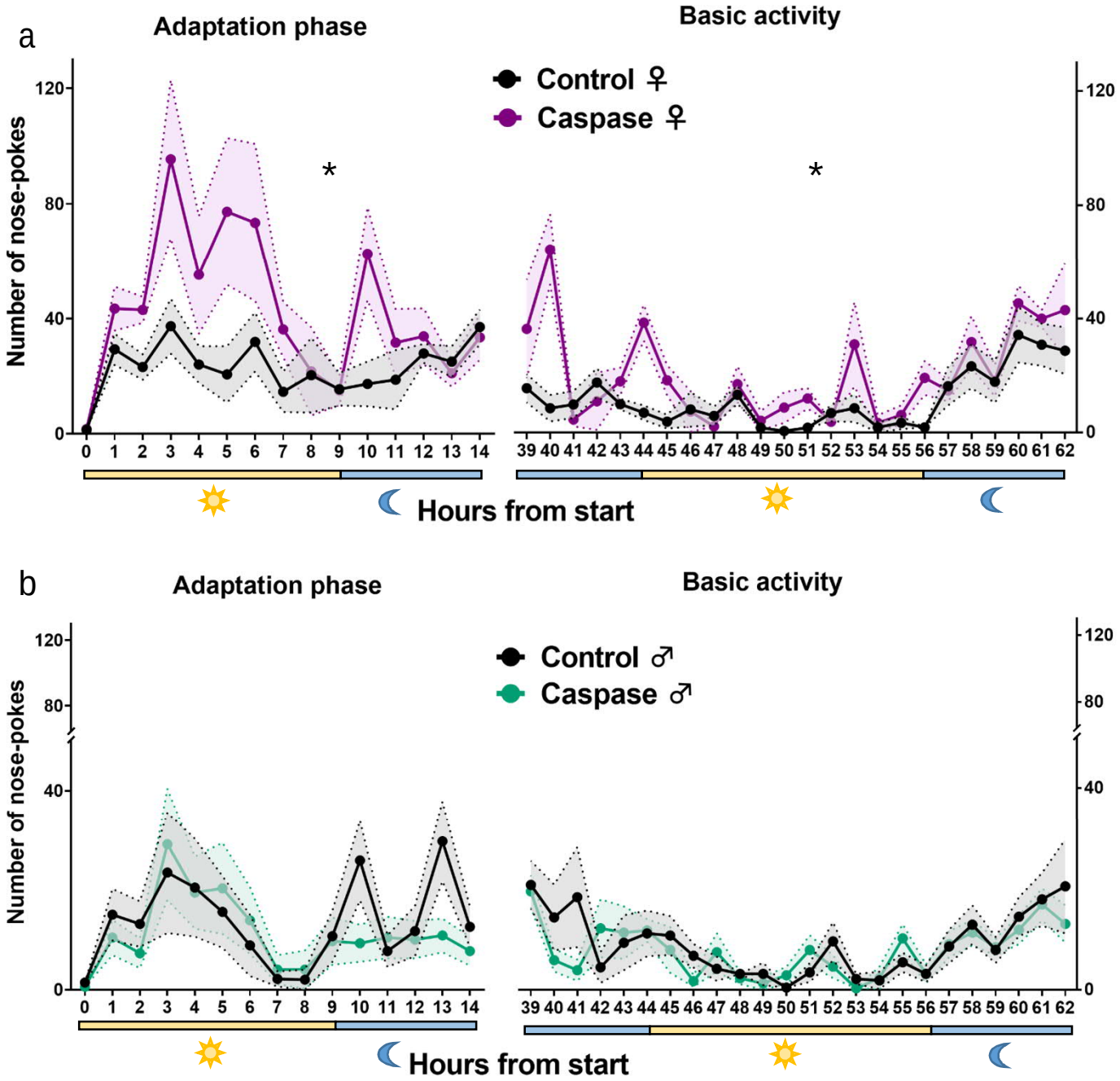

Figure 5. VTA^{Sst}-caspase female mice demonstrated an increased number of nose-pokes in the Intellicage system. Y-axis indicates the number of nose-pokes into the water-containing doors per h, X-axis shows the time after the beginning of the test. Yellow and blue bars beneath the graphs show light and dark phases, respectively. a. VTA^{Sst}–caspase females nose-poked more often in the Intellicage environment than the control females, suggesting higher activity during the adaptation (sex x treatment: $F(1,22) = 7.085$, $p=0.014$; ♀ *post-hoc* $p=0.004$) and after habituation to the new environment (sex x treatment: $F(1,22) = 8.043$, $p=0.010$; ♀ *post-hoc* $p=0.002$). Females were overall more active than males (sex: $F(1,22) = 27.329$, $p<0.001$). b. There was no difference between the male treatment groups. * $p < 0.05$ for the significance of the difference in overall activities (post-hoc test).

bioRxiv preprint doi: https://doi.org/10.1101/2023.01.06.522982; this version posted January 6, 2023. The copyright holder for this preprint (which was not certified by peer review) is the author/funder, who has granted bioRxiv a license to display the preprint in perpetuity. It is made available under aCC-BY-ND 4.0 International license.

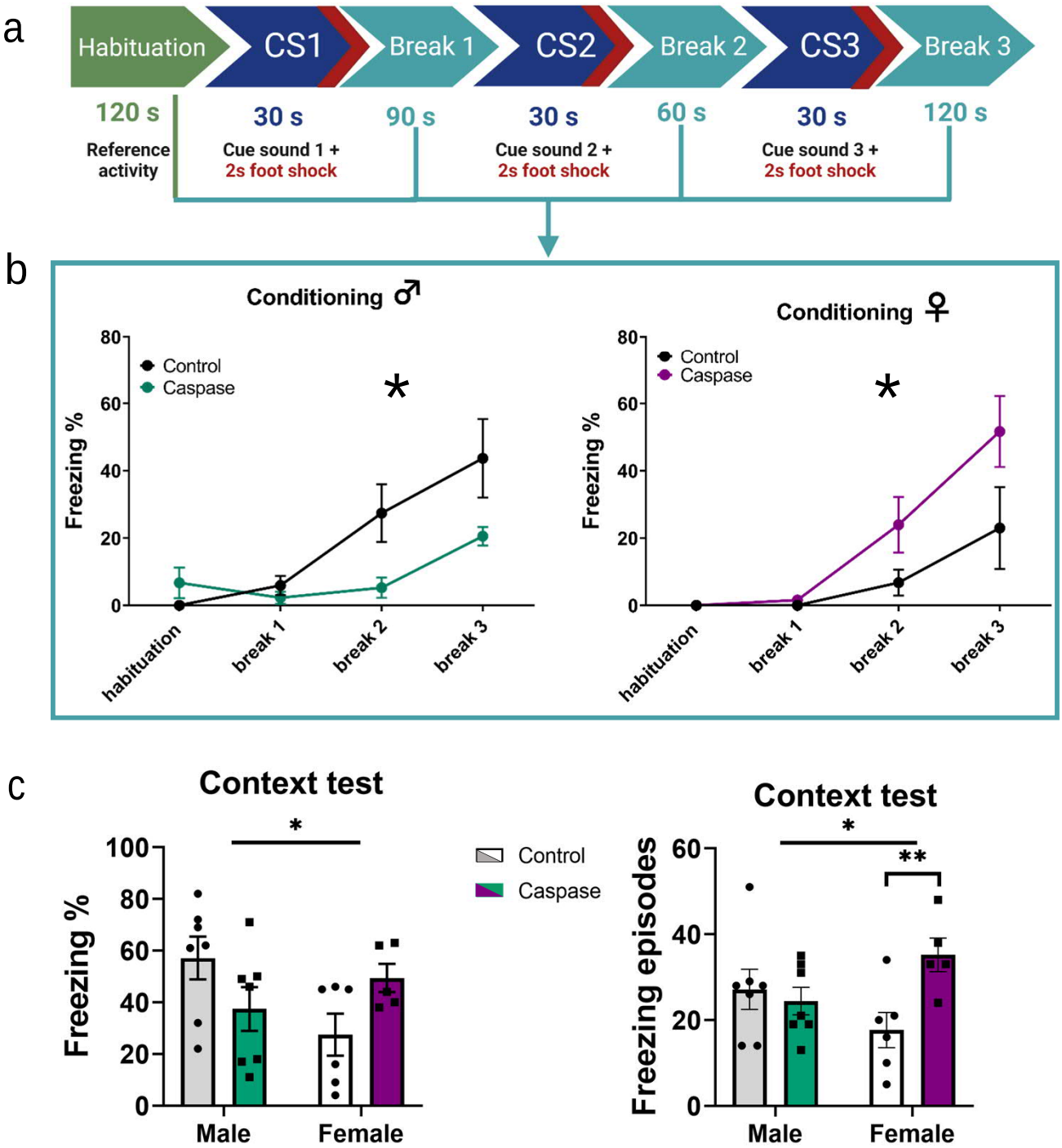

Figure 6. Deletion of VTA Sst neurons affected fear conditioning in a sex-dependent manner. a. Fear conditioning protocol during the acquisition phase (see methods). b. Graphs show per cent freezing (freeze time/total time) during breaks following the conditioning episodes (sex x treatment: $F(1,21)= 9.971$, $p=0.005$). The VTA^{Sst}-caspase males froze less during the breaks between foot shocks, whereas the VTA^{Sst}-caspase females, on contrary, froze more (*post hoc* males $p=0.036$, females $p=0.038$). c. A similar sex x treatment interaction ($F(1,21)= 6.602$, $p=0.018$ for freezing %; $F(1,21)= 6.102$, $p=0.022$ for freezing episodes) was observed in the context-associated fear memory retrieval test 9 days after the conditioning. The right graph shows that the VTA^{Sst}-caspase females froze more often, but, as seen in the left graph, not significantly longer (freezing %) than the control females (freezing episodes *post hoc* females $p=0.01$). Data are shown as mean ± SEM. *$p < 0.05$, **$p<0.01$.

bioRxiv preprint doi: https://doi.org/10.1101/2023.01.06.522982; this version posted January 6, 2023. The copyright holder for this preprint (which was not certified by peer review) is the author/funder, who has granted bioRxiv a license to display the preprint in perpetuity. It is made available under aCC-BY-ND 4.0 International license.

foot shocks when the sound was absent (breaks 1, 2 and 3; Fig. 6, S9b). Indeed, *post hoc* analysis confirmed that the VTA^{Sst-} males froze less than the control males (p=0.036) during the breaks between foot shocks, whereas the VTA^{Sst-} females froze more than the control females (p=0.038) (Fig. 6b). Interestingly, there were no differences between the VTA^{Sst+} and VTA^{Sst-} groups when the cue sound was on (Fig. S9b).

Further, we tested context-induced fear memory retrieval by placing the mice for 5 min in the same chamber, where they had received foot shocks 9 days earlier. Again, there was a similar sex*treatment interaction (p=0.018) in the percent freezing and freezing episodes (p=0.022; Fig. 6c) as we saw during the conditioning. Although *post hoc* tests did not show significant differences in the percent freezing between the treatment groups within sexes, the VTA^{Sst-} females showed more freezing episodes (p=0.01), meaning they froze more often but not significantly longer than the control females (Fig. 6c). Cue-induced retrieval or extinction after repeated cue presentations were not significantly affected by the deletion of the VTA Sst neurons, although the results showed similar sex-dependent trends as during the conditioning and context testing (Fig. S9c).

Deletion of VTA Sst neurons delays the onset of immobility in the forced-swim test

One of the non-sex-dependent changes in the behavioural performance of the mice lacking VTA Sst neurons was a delayed latency to the first immobility event in the forced-swim test (FST) (Fig. 7). Results showed that the VTA^{Sst-} mice struggled longer than the control group (p=0.031) and tended to spend less time immobile during the first 4 min of the test. As the tested animals were not exposed to any chronic stressor before the FST, the observed behavioural alteration might predominantly be related to a reaction to the acute unpredictable stressor.

bioRxiv preprint doi: https://doi.org/10.1101/2023.01.06.522982; this version posted January 6, 2023. The copyright holder for this preprint (which was not certified by peer review) is the author/funder, who has granted bioRxiv a license to display the preprint in perpetuity. It is made available under aCC-BY-ND 4.0 International license.

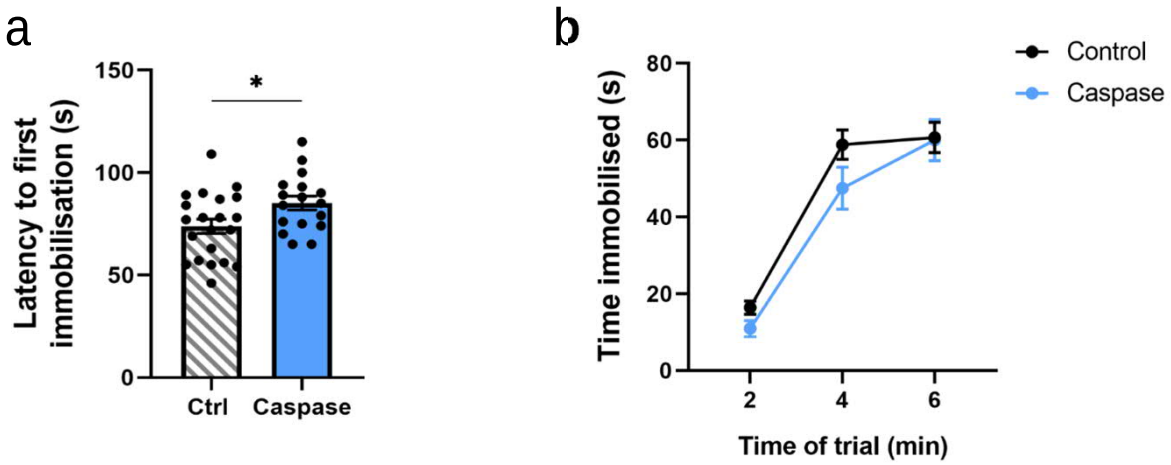

Figure 7. Delayed onset of immobility in the forced swim test in the VTA^{Sst}-caspase mice. a. VTA^{Sst}-caspase mice showed a longer latency to the first immobilisation event ($F(1,34) = 5.08$, $p = 0.031$), b. and a tendency for a shortened duration of immobilization (time x treatment: $F(2,68) = 1.938$, $p = 0.16$) especially in the first four min. Data are shown as mean ± SEM, and dots in panel a show individual data points. *$p < 0.05$.

bioRxiv preprint doi: https://doi.org/10.1101/2023.01.06.522982; this version posted January 6, 2023. The copyright holder for this preprint (which was not certified by peer review) is the author/funder, who has granted bioRxiv a license to display the preprint in perpetuity. It is made available under aCC-BY-ND 4.0 International license.

Deletion of VTA Sst neurons affected morphine sensitization, but not natural reward-related processing

Taking into account the previously shown ability of VTA Sst neurons to inhibit neighbouring DA cells (Nagaeva et al., 2020), it was important to find out whether drug and natural reward processing would be affected in VTA^{Sst-} animals. We chose morphine as the experimental substance since its rewarding potential is well known in rodents (Kuzmin et al., 1996; Martin et al., 1963) and its mechanism of action includes inhibition of VTA GABA cells resulting in excessive DA neuron firing by disinhibition (Johnson and North, 1992). There were no differences in the locomotor response to a single-dose morphine administration (20 mg/kg, i.p.) between the treatment groups (Fig. 8a), indicating that acute reaction to morphine was not affected in VTA^{Sst-} mice. However, we detected a significant enhancement in sensitization to locomotor activation by the second morphine challenge in the VTA^{Sst-} mice as compared to the control mice, 7 days after the first morphine injection (Fig. 8b).

As the natural reward to be tested, we chose sweetened drinking water but did not find any significant differences between the treatment groups in sucrose or saccharine consumption or preference over plain water (Fig. S10). We also designed two reward-based learning tasks for the Intellicage system aiming to assess alterations in prediction error processing (Schultz et al., 1997) and in punishment-resistant reward preference. For these tasks, the mice learned first to nose-poke in assigned corners to receive access to 0.3% saccharine in water. Each nose-poke to the saccharine door activated light informing that the saccharine will be available in 2 s. On the third day, when the task performance was stable, we either emptied the saccharine bottles or introduced 0.2-bar air puffs with a 25% probability at the end of the licking session (Radwanska and Kaczmarek, 2012). It is important to note that

bioRxiv preprint doi: https://doi.org/10.1101/2023.01.06.522982; this version posted January 6, 2023. The copyright holder for this preprint (which was not certified by peer review) is the author/funder, who has granted bioRxiv a license to display the preprint in perpetuity. It is made available under aCC-BY-ND 4.0 International license.

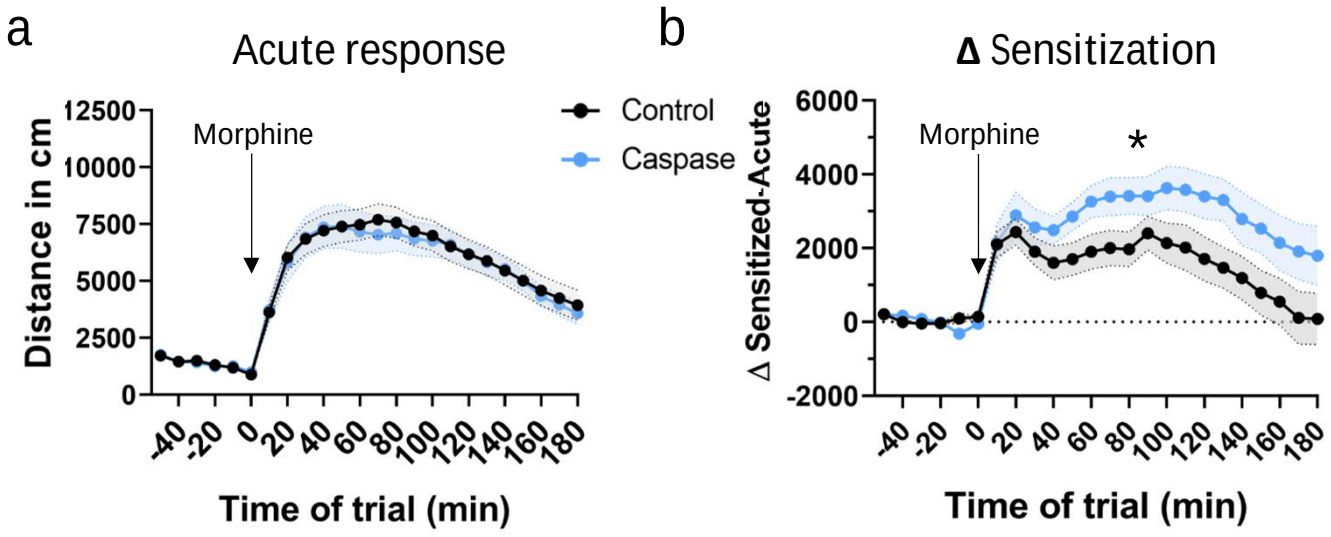

Figure 8. Increased morphine-induced locomotor sensitization in VTA^{Sst-} mice. Arrows indicate the time of morphine administration (20 mg/kg, i.p.) a. Acute treatment with morphine-induced similar hyperlocomotor response in both treatment groups (treatment: $F(1,32) = 0.034$, $p = 0.854$) b. Seven days after the first morphine injection, the response to the morphine challenge was enhanced and prolonged in the VTA^{Sst}-caspase mice as compared to controls [Treatment: $F(1,32) = 12.014$, $p = 0.002$; Time x treatment: $F(23,735) = 2.915$, $p = 0.024$]. Data are shown across 10 min time bins as means ± SEM. *$p < 0.05$.

bioRxiv preprint doi: https://doi.org/10.1101/2023.01.06.522982; this version posted January 6, 2023. The copyright holder for this preprint (which was not certified by peer review) is the author/funder, who has granted bioRxiv a license to display the preprint in perpetuity. It is made available under aCC-BY-ND 4.0 International license.

the two experimental tasks took place consecutively in the Intellicage allowing assessment of the re-learning rates after failed reward accesses.

The "prediction error" probing showed significant sex differences ($p<0.001$) and sex*treatment interaction ($p=0.043$) between the VTA^{Sst+} and VTA^{Sst-} groups (data not shown). However, further *post hoc* analysis separately for males and females did not show any significant differences between the treatments, but showed a tendency for the VTA^{Sst-} females to re-learn slower not to nose-poke anymore in an emptied saccharine bottle ($p=0.064$). For the next "punishment-resistant reward preference test", saccharine was re-introduced in new corners after being unavailable for 2 days and the mice had to re-learn the rules. Although there was a tendency of the VTA^{Sst-} male mice to be less active in nose-poking to saccharine corners in all phases of the re-learning/avoidance test (Fig. S11), we could not detect any statistically significant differences between the groups (see Table S1). Similarly, we did not detect any differences in reactions to air-puffs.

Delay discounting test revealed a sex-dependent, but not VTA Sst neuron-dependent difference

Even though we did not find any differences in the preference for saccharine or sucrose of various concentrations between the VTA^{Sst-} and control groups (Fig. S10), we observed an interesting sex-dependent behaviour in the delay discounting (DD) task (Mitchell, 2014) in Intellicage system. The delay discounting test, where mice learn to wait for a reward for increasing periods of time, showed a sex difference ($p=0.0239$) with significant dependence on the duration of the delay (sex*delay interaction $p<0.001$; Table S1). As shown in Fig. S12, for both male groups the longer delay to the saccharine delivery drastically decreased the number of licks to the saccharine bottle starting from a 4-s delay and dropped almost to nonexistent at a 5-s delay, while females were still willing to wait and lick. The delay-discounting test

bioRxiv preprint doi: https://doi.org/10.1101/2023.01.06.522982; this version posted January 6, 2023. The copyright holder for this preprint (which was not certified by peer review) is the author/funder, who has granted bioRxiv a license to display the preprint in perpetuity. It is made available under aCC-BY-ND 4.0 International license.

is usually interpreted as a measure of impulsivity, making male mice in our experiment more impulsive or less patient. However, we did not see any differences between the treatment groups within the sexes, suggesting that the deletion of the VTA Sst neurons did not affect impulsivity or readiness to wait for the reward.

Discussion

In the present study, we demonstrated that Sst neurons similarly to other neurons in the VTA can project outside the midbrain. In addition to their local inhibitory activity onto neighbouring DA cells (Nagaeva et al., 2020), VTA Sst neurons consistently project to at least five forebrain targets: alBNST, CeM, PVT, LH and VP. These projecting Sst neurons have a specific location in the anterolateral part of the VTA and they predominantly can express *Vglut2* or *Th*, or both of them. The existence of double positive Th+/Vglut2+ neurons is well established in the VTA of mice and rats by several studies (Li et al., 2013; Yamaguchi et al., 2015), reporting also that about 50% of these neurons lack mRNAs for the main DA markers (confirmed by our qPCR results). Some of these Th+/Vglut2+ neurons also fail to express detectable Th protein levels, and the majority of them were located in the medial VTA. However, we found here that Sst+/Th+/Vglut2+ projecting neurons were predominantly located in the anterolateral VTA, suggesting that they might represent a sizable proportion of the Vglut2+/Th-IR (immunoreactive) population described by Yamaguchi et al. (Yamaguchi et al., 2011), but still lack the possibility to produce and reuptake dopamine due to absence of *Ddc* and *Dat* expression.

Innervation pattern of the forebrain targets by the VTA Sst neurons resembles that found in Gad2-Cre mice, and to lesser extent that reported for the VTA Gad1+ efferents (Taylor et al., 2014). Moreover, in that study the expression patterns of *Th* and *Vglut2* in the VTA neurons projecting to the BNST, CeA, and VP were also quite similar to the patterns found in our study for VTA Sst neurons. However, projection

bioRxiv preprint doi: https://doi.org/10.1101/2023.01.06.522982; this version posted January 6, 2023. The copyright holder for this preprint (which was not certified by peer review) is the author/funder, who has granted bioRxiv a license to display the preprint in perpetuity. It is made available under aCC-BY-ND 4.0 International license.

repertoire of the Gad2+ VTA neurons was much wider than that of the VTA Sst neurons found by us, suggesting that the Sst promoter targets a more restricted population of the projecting neurons.

Taking into account mixed neurotransmitter nature of the VTA Sst neurons and the fact that *Sst* and *Gad2* can be expressed also in excitatory neurons (Phillips et al., 2022; Quina et al., 2020), it is logical to suggest that at least some of the targets found belong to the known VTA Glu neuron projections. For instance, some of the VTA Vglut2+ neurons have been shown to activate and inhibit VP neurons with the excitatory action to be more pronounced (Hnasko et al., 2012; Yoo et al., 2016). It is possible that the Sst projections described here represent a part of these Glu projections, as most of the VTA Sst projecting neurons in our experiments (72%) expressed *Vglut2*. However, physiological confirmation of the ability of the VTA Sst neurons to excite cells in their projection targets, e.g., using optogenetics, is needed for the conclusion about their Glu nature.

Similarly, optogenetic activation of the VTA neurons in Gad2-Cre mouse line showed functional inhibitory connection of these neurons with neurons in the CeM (Zhou et al., 2019), suggesting that the VTA Sst+ projections might constitute at least a part of the described VTA-CeM pathway. In the mentioned work, authors did not check out whether this pathway can also evoke excitatory postsynaptic currents, which it might be able to do as the VTA Sst-CeM neurons predominantly expressed *Vglut2* and *Gad2*, but not *Gad1* or *Vgat* (Fig. 4c). This remains to be confirmed in further research. Projections of the VTA GABA and Glu neurons to the LH has been shown to regulate wakefulness and sleeping behaviour (Yu et al., 2019). Taking into account that the Sst neurons projecting to the LH expressed *Vglut2* and sometimes *Gad1*/*Vgat*, it is plausible that in the work of Yu et al. a sizable population of the Sst neurons described here was responsible for the regulation. Interestingly, more recent work from the same laboratory identified, confirmed by our present findings,

bioRxiv preprint doi: https://doi.org/10.1101/2023.01.06.522982; this version posted January 6, 2023. The copyright holder for this preprint (which was not certified by peer review) is the author/funder, who has granted bioRxiv a license to display the preprint in perpetuity. It is made available under aCC-BY-ND 4.0 International license.

VTA Sst projections to the PVT and showed that this pathway regulates restorative sleep after stress (Yu et al., 2022). Here we, for the first time, to our knowledge, showed a direct connection between the VTA and alBNST through the Sst neurons.

Behavioural assessment of the deletion of the VTA Sst neurons revealed four major consequences: increased home-cage activity, altered response in the fear-conditioning, enhanced locomotor sensitization to the second dose of morphine and prolonged struggle during the inescapable stress of forced swimming. The first two changes showed also a significant sexual dimorphism.

Regarding the home-cage activity, it is well known that females are more active than males in the Intellicage environment where they are group-housed (Pernold et al., 2021, 2019), as we also observed (Table S1). Interestingly, the deletion of the VTA Sst neurons resulted in a further increase of the home-cage activity exclusively in the female mice (Fig. 5). The activity change was not associated with the novelty of the environment: it was consistent throughout the experiment and after several days of adaptation. Circadian patterns in single-housed animals determined during 3-day access to free-running wheels failed to differ between VTA^{Sst-} and control animals (Fig. S7). In addition, there was no change in locomotor activity, as the distance travelled in the open field was similar between the two treatment groups. Our data suggest that deletion of the VTA Sst neurons resulted in a specific increase in home-cage activity and only in group-housed female mice. The underlying mechanism of this distinct change needs further investigation.

Although several of the VTA Sst neuron projection targets, like the BNST (Lebow and Chen, 2016), CeM (Shackman and Fox, 2016) and PVT (Kirouac, 2021) are involved in the brain anxiety network, we did not see any significant differences in the anxiety-like bahaviours in VTA^{Sst-} mice. This was measured in a light-dark box, elevated plus maze, novelty-suppressed feeding tests (Fig. S8) or reaction to the air-

bioRxiv preprint doi: https://doi.org/10.1101/2023.01.06.522982; this version posted January 6, 2023. The copyright holder for this preprint (which was not certified by peer review) is the author/funder, who has granted bioRxiv a license to display the preprint in perpetuity. It is made available under aCC-BY-ND 4.0 International license.

puffs (Fig. S11), and suggests the VTA Sst neurons might not be involved in innate threat and avoidance of elevated or brightly lit areas. On the contrary, our data indicated that these neurons could be meaningful for the responses to inescapable acute stressors, such as freezing after unexpected foot shock (fear-conditioning acquisition phase) or struggling when dipped into water (forced swim test).

Significant, but opposite changes in the reaction to the foot shock in males vs. females (Fig. 6b) was another interesting effect of VTA Sst neuron deletion, which again emphasizes differences in the VTA Sst+ projections or their functional outcome depending on the sex. It is important to note, that our data do not exclude the possibility that the nociceptive reaction itself was altered in the VTA^{Sst-} animals explaining why VTA^{Sst-} males froze less and VTA^{Sst-} females froze more than controls in response to the foot shock. Interestingly, a recent study described a pathway from the laterodorsal tegmentum (LDTg) via VTA to the basolateral amygdala, inhibition of which reduced unconditioned freezing response to foot shocks in male mice, similar to what we observed in the VTA^{Sst-} males (Broussot et al., 2022). Unfortunately, results on females were not reported in that study. Our results emphasize the importance of conducting experiments on both sexes, especially in case of aversive-stimuli reactions (see also Cover et al., 2014). Fear-conditioning test highlighted an interesting feature of the VTA Sst neuron function: these neurons were important for the contextual fear memory formation/retrieval, but not for the sound cue-associated responses, likely relating to differential processing of these two modalities of conditioned stimuli.

The fact that many brain regions receiving VTA Sst neuron projections belong to the extended amygdala suggests the involvement of these neurons in the action of addictive substances, such as opioids and alcohol (Koob et al., 2014a, 2014b). We did not see any differences in locomotor responses to acute morphine administration (Fig. 8a), indicating that the opioid stimulating effect was not

bioRxiv preprint doi: https://doi.org/10.1101/2023.01.06.522982; this version posted January 6, 2023. The copyright holder for this preprint (which was not certified by peer review) is the author/funder, who has granted bioRxiv a license to display the preprint in perpetuity. It is made available under aCC-BY-ND 4.0 International license.

affected by the deletion of the VTA Sst neurons. This is consistent with the data on rats, where morphine actions on VTA DA neurons could be prevented by silencing GABA neurons in the rostromedial tegmental (RMtg, also called the tail of VTA) (Jalabert et al., 2011), which might be more meaningful for the acute disinhibitory action of opioids on VTA DA neurons. More importantly, we did observe that after the second morphine administration 7 days later, the VTA^{Sst-} mice of both sexes demonstrated robustly increased locomotor sensitization, suggesting that the VTA Sst neurons normally limit the sensitization to opioids. This might be linked to morphine-induced adaptation of $GABA_A$ receptor-mediated transmission onto VTA DA neurons (Nugent et al., 2007), which would be missing from intra-VTA synapses of Sst neurons in caspase-treated VTA^{Sst-} mice. This remains to be studied, especially since VTA Sst neurons are also projection neurons and can have long-distance circuit effects.

Interestingly, similar increase in opioid sensitization resulting in higher morphine preference afterwards (Shaham et al., 1992) is often observed as a consequence of stressful events (Kalivas et al., 1986; Leyton and Stewart, 1990), also of emotional nature (Kuzmin et al., 1996). Since it also has been shown that deletion of the VTA Sst neurons disrupt normal restorative sleep after social defeat stress (Yu et al., 2022), it is possible to speculate that in both cases the VTA Sst neurons are involved in the adaptive changes of the VTA circuit which might occur only during sleep. The fact that morphine challenge in our experiments was done 7 days later also speaks in favour of this. However, further research is needed to elucidate the actual mechanism of such adaptations.

Overall, our study has demonstrated that Sst neurons in the VTA, like in other brain areas, constitute a population of projection neurons, which together can form a brain-wide somatostatinergic system, as has been recently proposed (Viollet et al., 2008). Our data suggest sex-dependent differences in VTA Sst-neuron effects on

bioRxiv preprint doi: https://doi.org/10.1101/2023.01.06.522982; this version posted January 6, 2023. The copyright holder for this preprint (which was not certified by peer review) is the author/funder, who has granted bioRxiv a license to display the preprint in perpetuity. It is made available under aCC-BY-ND 4.0 International license.

behaviour, which together with the restricted location within mouse VTA that we established here would make possible their targeted manipulation in optogenetic and electrophysiological studies on behaving animals in both sexes. Thus, our findings lay the base for more advanced experiments on the role of VTA Sst neurons in, e.g., addictions, depression and stress adaptation.

bioRxiv preprint doi: https://doi.org/10.1101/2023.01.06.522982; this version posted January 6, 2023. The copyright holder for this preprint (which was not certified by peer review) is the author/funder, who has granted bioRxiv a license to display the preprint in perpetuity. It is made available under aCC-BY-ND 4.0 International license.

Materials & Methods

Animals. All experimental procedures were performed on male and female mice of either homozygous Sst-IRES-Cre (Sst$^{tm2.1(cre)Zjh}$/J) or heterozygous genotype resulted from cross-breeding of Sst-IRES-Cre (Sst$^{tm2.1(cre)Zjh}$/J) strain with Ai14 tdTomato reporter strain (B6.Cg-Gt(ROSA)26Sor$^{tm14(CAG-tdTomato)Hze}$/J). Two female Th-EGFP mice (Tg(Th-EGFP)DJ76Gsat) of the age P140 were used for the qPCR experiment on the dopamine neurons. Animals were group-housed in individually ventilated cages (IVC)-cages (Tecniplast Green Line GM500) under 12:12 h light/dark cycle (lights on 6 am – 6 pm) with *ad libitum* access to food (Global Diet 2916C, pellet 12 mm, Envigo) and water, unless otherwise indicated in the corresponding method section. Cages were equipped with bedding (500 ml aspen chips 5 x 5 x 1 mm, 4HP, Tapvei), nesting material (aspen strips, PM90L, Tapvei) and a clear handling tube (10 cm length, 5 cm diameter). Animal experiments were authorized by the National Animal Experiment Board in Finland (Eläinkoelautakunta, ELLA; license numbers: ESAVI/1172/04.10.07/2018 and ESAVI/1218/2021).

Tracing. The mice were anesthetized with a mixture of isoflurane (4% for induction, 0.5 – 2% for maintenance; Vetflurane, Virbac, Carros, France) and air (flow rate 0.8 – 1 l/min), after which they were placed into a stereotaxic frame (Kopf Instruments, Tujunga, CA, USA). Before opening incision on the scalp, iodopovidone was applied on the surgical region, and lubricative eye gel applied to prevent corneal damage.

For the anterograde tracing studies, stereotaxic coordinates AP: -3.3 ML: ± 0.3 DV: -4.5 mm relative to bregma were used for the VTA, based on the Mouse Brain Atlas (Franklin and Paxinos, 2007) and verified with dye injections. A unilateral injection of 200 nl of AAV2/8-Cag-Flex-Myr-eGFP viral construct (lot 4x1012 genome copies/ml; AAV 319 lot, Neurophotonics Center, CERVO Brain Research Centre,

bioRxiv preprint doi: https://doi.org/10.1101/2023.01.06.522982; this version posted January 6, 2023. The copyright holder for this preprint (which was not certified by peer review) is the author/funder, who has granted bioRxiv a license to display the preprint in perpetuity. It is made available under aCC-BY-ND 4.0 International license.

Quebec, Canada) was made with a flow rate of 0.1 µl/min. A precision pump system (KD Scientific, Holliston, MA, USA) was used to control the injection rate.

For the retrograde tracing, the following stereotaxic coordinates were used (mm relative to bregma): for the BNST, AP: -0.1 ML: ±0.9 DV: -4.2; for the CeA, AP: -1.5 ML: ±2.6 DV: -4.7; for the LH, AP: -1.4 ML: ±1.1 DV: -5.3; for the PVT, AP: -1.5 ML: ±0.1 DV: -3.2; for the VP, AP: +0.6 ML: ±1.3 DV: -5.4. For each animal, a 600-nl unilateral injection of 1:1 mixture of green retrobeads (1:10 dilution in dH_2O, Lumafluor Inc., Durham, NC, USA) and pAAV2-hSyn-DIO-EGFP retrograde virus construct ($7.6x10^{12}$ genome copies/ml; 50457-AAVrg, Addgene, Watertown, MA, USA) was made with a flow rate of 1.0 µl/min. Retrobeads were used only for marking the injection site and not considered in the backtracing analysis. After the surgeries the mice were administered 5 mg/kg carprofen (s.c. Norocarp Vet 50 mg/ml, Norbrook Laboratories Ltd, Newry, Northern Ireland) for postoperative analgesia, and were let to recover from anesthesia in a 37°C incubator until ambulatory. A recovery period of at least 3 weeks was allowed before further procedures.

Mice were anaesthetized with pentobarbital (200 mg/kg i.p., Mebunat, Orion Pharma, Espoo, Finland) and perfused transcardially with cold 1xPBS solution followed by 4% paraformaldehyde solution. After overnight in the same fixative solution, brains were transferred to 30% sucrose until sinking (at least 48 h). The brains were then frozen on dry ice and stored at -80°C until sectioned. For the anterograde tracing, 80-µm coronal sections were cut throughout the brain, and for the retrograde tracing 40-µm coronal sections from the injection site and the VTA were cut with cryostat (CM3050S, Leica Biosystems, Wetzlar, Germany).

To enhance the fluorescence signal of the antero-traced axons, anti-GFP immunostaining was performed. The sections were washed at room temperature in

bioRxiv preprint doi: https://doi.org/10.1101/2023.01.06.522982; this version posted January 6, 2023. The copyright holder for this preprint (which was not certified by peer review) is the author/funder, who has granted bioRxiv a license to display the preprint in perpetuity. It is made available under aCC-BY-ND 4.0 International license.

1x PBS (5 min, 3 times), and blocked with 1% bovine serum albumin (BSA; Sigma Aldrich, Saint Louis, MO, USA) with 0.3% Triton X-100 (BDH Laboratory Supplies, Poole, UK) in 1x PBS for 1 h at room temperature. The sections were then incubated with the primary antibody (chicken anti-GFP 1:800 in blocking solution; ab13970, Abcam, Cambridge, UK) overnight at 4°C, washed with 1x PBS (5 min, 3 times) and incubated with the secondary antibody (goat anti-chicken with Alexa Fluor 488 1:800 in blocking solution; ab150169, Abcam) for 2 h at room temperature. Sections were then washed once more with 1x PBS (5 min, 3 times), mounted on microscope slides, and coverslips were applied with Vectashield mounting medium (Vector Laboratories, Burlingame, CA, USA).

Imaging was performed with Zeiss Axio Imager Z2 (Zeiss AG, Oberkochen, Germany) with 10x air objective in tiles mode. Injection site was considered as successful if 90% of GFP-positive infected cell bodies were located within the VTA area. Sst nature of the infected cells was also confirmed by red inbuilt signal of tdTomato. Anterograde targets of the projecting cells were considered as positive by having maximum brightness due to GFP-expressing axonal arborization. The conclusion about the constancy of the projection target was made according to hierarchical clustering results produced by *hclust* function implemented in R programming environment (https://www.rdocumentation.org/packages/stats/versions/3.6.2/topics/hclust). Retrogradely traced neurons within the VTA were counted as positive by having clear co-expression of the inbuilt tdTomato signal and the GFP signal caused by the viral infection.

Electrophysiology and single-cell qPCR. To define electrophysiological and molecular profiles of the VTA projecting Sst neurons we combined backtracing with current-clamp recordings and single-cell qPCR. Backtracing was performed as described above (see Tracing section) on P60-P90 old Sst-IRES-Cre homozygous

bioRxiv preprint doi: https://doi.org/10.1101/2023.01.06.522982; this version posted January 6, 2023. The copyright holder for this preprint (which was not certified by peer review) is the author/funder, who has granted bioRxiv a license to display the preprint in perpetuity. It is made available under aCC-BY-ND 4.0 International license.

animals of both sexes. Electrophysiology was done after at least 1 month of recovery as described previously (Nagaeva et al., 2020) with some modifications. Shortly, mice were perfused with ice-cold constantly oxygenated NMDG-based cutting solution. Coronal VTA sections of 225 µm thickness were cut in the same solution using vibrotome HM650V (Thermo Scientific, Waltham, MA, USA) and transferred to the constantly oxygenated 33°C HEPES-ACSF solution for 15 min recovery and then remained in the same solution at room temperature until the end of the experiment (~ 3 h). For the injection site verification, sections were cut in the same way as the VTA sections and checked immediately with the epifluorescence microscope BX51WI (Olympus, Tokyo, Japan).

Electrophysiological registration of the firing patterns was performed in the same conditions as previously described (Nagaeva et al., 2020) to allow the data alignment. Backtraced Sst GFP-positive cells were identified with an epifluorescence microscope BX51WI and sCMOS camera Andor Zyla 5.5 (Oxford Instuments, Oxford, UK). Whole-cell current-clamp recordings were made using 3–5 MΩ borosilicate glass electrodes filled with 1-2 µL of intracellular solution (IS) (containing in mM): 130 K-gluconate, 6 NaCl, 10 HEPES, 0.5 EGTA, 4 Na2-ATP, 0.35 Na-GTP, 8 Na2-phosphocreatine (pH adjusted to 7.2 with KOH, osmolarity ~285 mOsm). 1 U/µL TaKaRa RNAse inhibitor (Takara, Shiga, Japan) was added before each experiment. Liquid junction potential (+12 mV) was not corrected during recordings.

All electrophysiological experiments were made with an Multiclamp 700B amplifier (Molecular Devices, USA) filtered at 2 kHz, and recorded with 10 kHz sampling rate using pClamp 10 software (Molecular Devices). After achieving whole-cell configuration in voltage-clamp mode (−70 mV), cell capacitance was determined by the 'Membrane Test' feature of the Clampfit software and the amplifier was then switched to current-clamp mode. Depolarized cells with RMP higher than −50 mV

bioRxiv preprint doi: https://doi.org/10.1101/2023.01.06.522982; this version posted January 6, 2023. The copyright holder for this preprint (which was not certified by peer review) is the author/funder, who has granted bioRxiv a license to display the preprint in perpetuity. It is made available under aCC-BY-ND 4.0 International license.

were excluded. For measuring passive and active membrane properties, neurons were injected with 800-ms current steps with 10 pA increments, resulting in the membrane voltage fluctuation from -120 mV to the saturated level of firing. In addition, shorter protocol from 0 pA with 1 pA increment was applied for better identification of the action potential threshold and shape. All recordings were performed with intact GABAergic and glutamatergic transmission (i.e. no pharmacological agents were added to the aCSF).

Extraction of mRNA. After firing pattern registration, cell body was immediately sucked into the glass electrode with negative pressure and expelled onto a 1.1 µl drop of the ice-cold lysis buffer (0.1% Triton X-100, 2 U/µl TaKaRa RNAse inhibitor, 0.5 µM Oligo-dT_{30} primer, 11.5 mM dithiothreitol and 2.3 mM of dNTP mix) placed on the wall of cold RNAse-free PCR tube, spun down and immediately frozen in dry ice. All samples were stored at −80°C until the reverse transcription step.

Reverse transcription (RT) and pre-amplification. Frozen samples were thawed at 72°C for 3 min. 2 µl of RT mix (1x SuperScript IV buffer, 18 U/µl SuperScript IV reverse transcriptase (Thermofisher Scientific, USA), 3.6 µM TSO-chimera primer, 6 mM MgCl2, 0.8 M betaine and 1.5 U/µl TaKaRa RNAse inhibitor) were added to each sample, mixed gently, spun down and then incubated in the thermocycler (52°C - 10 min, [60°C - 1 min, 52°C - 1 min] x 10 times, 80°C - 20 min). For further cDNA amplification, 20 µl of PCR mix [1xPlatinum SuperFi II master mix, 0.5 µM PCR1 primer, 111 nM dNTP mix] were gently pipetted to each sample, which then underwent the following thermocycler program (98°C - 30 s, [98°C - 10 s, 60°C - 11 s, 72°C - 6 min] x 25 times, 72°C - 5 min).

qPCR analysis. The synthesized cDNA samples were diluted to the concentration range 100-300 ng/µl with sterile DNAse free water. Samples were

bioRxiv preprint doi: https://doi.org/10.1101/2023.01.06.522982; this version posted January 6, 2023. The copyright holder for this preprint (which was not certified by peer review) is the author/funder, who has granted bioRxiv a license to display the preprint in perpetuity. It is made available under aCC-BY-ND 4.0 International license.

then amplified with PowerUp™ SYBR™ Green Master Mix (Applied Biosystems, USA) following the instructions of the manufacturer. Quantitative PCR (qPCR) was performed using LightCycler® 480 II system (Roche Diagnostics, Switzerland) with the following conditions: UDG (uracil-DNA glycosylase) activation 2 min at 50°C, pre-incubation 2 min at 95°C, followed by amplification steps 40 cycles of 15 s at 95°C and 1 min at 60°C with melting curve. Expression of the following genes were determined. *Sst*, *Th*, *Egfp*, *Nos1, Ddc, Gad1*, *Gad2*, *Slc17a6* (*Vglut2*), *Slc32a1* (*Vgat*), and *Slc6a3* (*Dat*). The primer sequences were obtained from the PrimerBank (https://pga.mgh.harvard.edu/primerbank/index.html). Primers were ordered from Metabion (Metabion International AG, Germany) and actual sequences are listed in table below this section. Every run included a negative control, a positive control (bulk cDNA from mouse visual cortex) and blank (H_2O). The qPCR reactions were performed in triplicate for each sample, and their averages were used for Ct values. The Ct values of EGFP were used to normalize expression by delta Ct method. The relative expression was calculated based on the delta Ct values. Resulting values were then normalized with $\log_{10}$ transformation for the clustering procedure performed as described in the “Tracing” part.

PRIMERS LIST	
cDNA synthesis and amplification	
Oligo-dT30	5'-AAG CAG TGG TAT CAA CGC AGA GTA CT30AT-3'
TSO-chimera	5'-AAG CAG TGG TAT CAA CGC AGA GTA CAT ggg-3'
PCR1	5'-AAG CAG TGG TAT CAA CGC AGA GT-3'

qPCR		
Gene	forward	reverse
Sst	5'-ACC GGG AAA CAG GAA CTG G-3'	5'-TTG CTG GGT TCG AGT TGG C-3'
Slc32a1 - Vgat	5'-ACC TCC GTG TCC AAC AAG TC-3'	5'-CAA AGT CGA GAT CGT CGC AGT-3'
Slc17a6 - Vglut2	5'-TGG AAA ATC CCT CGG ACA GAT-3'	5'-CAT AGC GGA GCC TTC TTC TCA-3'
Th	5'-GTC TCA GAG CAG GAT ACC AAG C-3'	5'-CTC TCC TCG AAT ACC ACA GCC-3'
Slc6a3-Dat	5'-AAA TGC TCC GTG GGA CCA ATG-3'	5'-GTC TCC CGC TCT TGA ACC TC-3'

bioRxiv preprint doi: https://doi.org/10.1101/2023.01.06.522982; this version posted January 6, 2023. The copyright holder for this preprint (which was not certified by peer review) is the author/funder, who has granted bioRxiv a license to display the preprint in perpetuity. It is made available under aCC-BY-ND 4.0 International license.

Ddc	5'-TAGCTGACTATCTGGATGGCAT-3'	5'-GTCCTCGTATGTTTCTGGCTC-3'
Gad1	5'-CAC AGG TCA CCC TCG ATT TTT-3'	5'-ACC ATC CAA CGA TCT CTC TCA TC-3'
Gad2	5'-TCC GGC TTT TGG TCC TTC G-3'	5'-ATG CCG CCC GTG AAC TTT T-3'
EGFP	5'-AGT CCG CCC TGA GCA AAG A-3'	5'-TCC AGC AGG ACC ATG TGA TC-3'
Nos1	5'-CTGGTGAAGGAACGGGTCAG-3'	5'-CCGATCATTGACGGCGAGAAT-3'

Caspase experiments. For the caspase manipulations, Sst-tdTomato heterozygous male and female mice of the age P60-P75 (on the injection day) were used. All the injection procedures were similar to those described in the "Tracing" part of the Methods. Slightly modified coordinates for the VTA were used, aiming at the antero-lateral Sst sub-population (Nagaeva et al., 2020) and based on the results of the retrograde tracing to hit the majority of the projecting VTA Sst neurons (mm relative to bregma): AP: -3.1, ML: ±0.7, DV: -4.6. 600-nl bilateral injections of 1:1 mixture of AAV1/2-DIO-taCasp3-TEV ($3x10^{12}$ genome copies/ml, a kind gift from professor William Wisden) and AAV2/8-CAG-Flex-Myr-eGFP ($4x10^{12}$ genome copies/ml; Neurophotonics Center, CERVO Brain Research Centre, Quebec, Canada) viral constructs, or 1:1 dH_20 dilution of AAV2/8-CAG-Flex-Myr-eGFP for the controls, were made with a flow rate of 0.1 µl/min. After surgery, mice had a recovery period of 4 weeks before the behavioural tests.

Confirmation of the deletion of VTA Sst neurons was made after the end of all behavioural experiments. Mice were perfused as described in the "Tracing" methods section. Forty-µm-thick coronal sections containing the VTA area were made and imaged with the epifluorescence microscope. Number of the GFP-expressing cells were counted in the control and caspase groups and compared. The caspase brains where injection site did not reach the VTA, were too lateral, or too medial were excluded from the analysis (4 mice from cohort 1; 2 from cohort 2, and

bioRxiv preprint doi: https://doi.org/10.1101/2023.01.06.522982; this version posted January 6, 2023. The copyright holder for this preprint (which was not certified by peer review) is the author/funder, who has granted bioRxiv a license to display the preprint in perpetuity. It is made available under aCC-BY-ND 4.0 International license.

5 mice from the "Intellicage cohort"). Subjective exclusion was performed by two independent researchers.

Behavioural experiments

General description: 17 (9 male, 8 female) VTA^{Sst-} and 21 (10 male, 11 female) VTA^{Sst+} control mice underwent a battery of behavioural tests to study reward- and anxiety-related behaviours. Experiments were performed in the morning between 7 am and 1 pm. Mice were always habituated to the testing room 45 – 60 min prior the experiment. Arenas were cleaned thoroughly with water between animals. Researchers conducting the experiments were blinded to the treatment group of the animals. Mice were initially group-housed, but then single-housed (including 7 days habituation) for conducting the novelty-suppressed feeding, sucrose preference, running wheel activity and morphine sensitization tests (see the schematic timeline below). To reduce stress from the injection, mice underwent a 5-day habituation routine prior to morphine injections as described before (Elsilä et al., 2022)

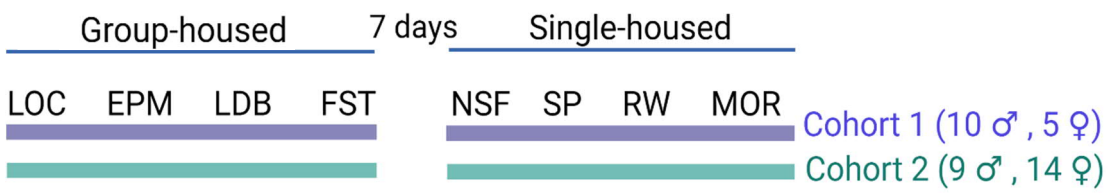

Novelty-induced locomotor activity (LOC) and morphine sensitization (MOR). The experiment was performed as described previously (Vashchinkina et al., 2012). Shortly, mice were released one by one in the novel open arena (36 x 19 x 20 cm). Distance moved was recorded during 60 min with EthoVision XT 10 tracking equipment (Noldus, Netherlands). Illumination in the room was approximately 50 lux.

bioRxiv preprint doi: https://doi.org/10.1101/2023.01.06.522982; this version posted January 6, 2023. The copyright holder for this preprint (which was not certified by peer review) is the author/funder, who has granted bioRxiv a license to display the preprint in perpetuity. It is made available under aCC-BY-ND 4.0 International license.

For morphine-sensitization, each mouse was habituated to the arena for 60 min after which it received a morphine injection (20 mg/kg, i.p.) and were immediately placed back in the arena. Mice remained in the arena for 3 h, and locomotor behaviour was monitored using EthoVision (induction day). After the testing, mice were put back to their home cage. Mice were challenged with a morphine injection 7 days later, and the experiment was repeated in the same context (challenge day). Sensitization to the morphine-enhanced locomotor activity was calculated as difference of distance moved on the challenge day minus distance moved on the induction day.

Elevated plus maze (EPM). The elevated plus maze was made out of gray plastic and consisted of a central platform (5 x 5 cm), from which two open arms and two enclosed arms (5 x 40 x 20 cm) extended at an elevation of 50 cm from the floor (Lister R.G., 1987). The light intensity of the closed arms were 10 lux and open arm 200 lux. The mouse was placed on the central platform facing a closed arm and allowed free exploration of the maze for 5 min. Distance moved and time spent in different arms was recorded with EthoVision. Time spent in the open arm was calculated as the percentage from the total time spent in all arms.

Light-dark box (LDB). The test was performed in an open-field arena (43.2 x 43.2 x 30.5 cm, ENV-515, Med Associates Inc., St. Albans, VT) equipped with infrared light transmitters and sensors detecting horizontal and vertical activity. The dark insert (non-transparent for visible light) was used to divide the arena into two equally sized compartments. An open door (width of 5.5cm and height of 7 cm) in the wall of the insert allowed the animal to freely move between compartments. Illumination in the light compartment from bright ceiling lights was ~ 200 lm. The animal was released in the door, head facing the dark compartment and allowed to explore the arena for 5 min. Distance moved and time spent in different

bioRxiv preprint doi: https://doi.org/10.1101/2023.01.06.522982; this version posted January 6, 2023. The copyright holder for this preprint (which was not certified by peer review) is the author/funder, who has granted bioRxiv a license to display the preprint in perpetuity. It is made available under aCC-BY-ND 4.0 International license.

compartments were recorded by the system. Time spent in the light compartment was calculated as the percentage from the total time spent in both compartments.

Forced swim test (FST). The mouse was placed for 6 min in a glass beaker (diameter 15 cm, height 25 cm) filled with 3 L of water at 23 ± 1°C (Procaccini et al., 2011). Three visually isolated mice were recorded simultaneously using a digital video camera. Latency to the first immobility and time of total immobility (i.e. passive floating, when an animal was motionless and only doing slight movement with a tail or one hind limb, in contrast to struggling, climbing or swimming with all four paws) were measured manually in 2-min intervals by a blinded researcher.

Novelty-suppressed feeding (NSF). Mice were single-housed and food-restricted for 14 h before testing to motivate food-seeking behaviour. Water was given *ad libitum*. Mice were tested in an open arena (50 x 50 x 28 cm) at an illumination of 200 lux. A lid from a 50-mL falcon tube was placed in the middle of the arena that contained a small amount of moist food. The mouse was released next to the wall, and its behaviour was recorded using EthoVision. Latency until the mouse started eating (i.e. eating for more than 5 s) was monitored manually by a researcher, after which the trial was terminated (maximum cut-off point 10 min). The mouse was returned to its home cage, where it was again presented with a small amount of moist food. Latency until first in-cage eating was monitored as previously. This was done to account for possible differences in hunger between animals.

Sucrose preference test (SP). Two-bottle choice sucrose preference test was carried out for 7 days (Lainiola et al., 2019). Mice were single-housed in larger IVC-cages allowing the use of two drinking bottles. Drinking bottles were weighted daily at 10:00 am to monitor consumption. The position of the water and sucrose bottles were changed every day to avoid the development of side preference. Mouse body

bioRxiv preprint doi: https://doi.org/10.1101/2023.01.06.522982; this version posted January 6, 2023. The copyright holder for this preprint (which was not certified by peer review) is the author/funder, who has granted bioRxiv a license to display the preprint in perpetuity. It is made available under aCC-BY-ND 4.0 International license.

weights were measured before and after the start of the experiment. Sucrose concentrations were based on an earlier study analysing sucrose preference in C57 mice (Sclafani, 2006) and were increased as follows: 0.1% (two days), 0.5% (two days) and 1% sucrose (three days). Average was taken for each sucrose concentration. Sucrose preference was calculated as a percentage of sucrose consumption out of the total fluid intake.

Circadian rhythm of wheel running (RW) activity. To measure voluntary wheel running activity, free-running wheels (MedAssociates Inc.,) was placed in the IVC cage of a single-housed mouse. Rotation of the wheel by the mouse was transmitted as electronic signal wirelessly to a hub and recorded on the Wheel Manager software. Data was exported every morning, and running wheels were checked for proper functioning. Voluntary running wheel activity was followed for 3 days, of which the first day was considered as habituation followed by two days of basal activity. Ten mice, which did not use the running wheel and ran <100 rotations over a course of 3 days, were excluded from the analysis.

IntelliCage (IC). A separate “Intellicage cohort” of 15 males and 16 females were subcutaneously injected with RFID transponders (Planet ID GmbH, Germany) for individual identification. The IntelliCage by NewBehaviour (TSE Systems, Germany) is an apparatus designed to fit inside a large cage (610 x 435 x 215 mm, Tecniplast 2000P). The apparatus itself provides four recording chambers that fit into the corners of the housing cage. Access into the chambers was provided via a tubular antenna (50 mm outer and 30 mm inner diameter) reading the transponder codes. The chamber contains two openings of 13 mm diameter (one on the left, one on the right), which gave access to drinking bottles. These openings are crossed by photo beams recording nose-pokes of the mice and the holes can be closed by motorized doors. Four triangular red shelters (Tecniplast, Buguggiate, Italy) were placed in the middle of the IntelliCage and used as sleeping quarters and as a stand

bioRxiv preprint doi: https://doi.org/10.1101/2023.01.06.522982; this version posted January 6, 2023. The copyright holder for this preprint (which was not certified by peer review) is the author/funder, who has granted bioRxiv a license to display the preprint in perpetuity. It is made available under aCC-BY-ND 4.0 International license.

to reach the food. The floor was covered with a thick (2-3 cm) layer of bedding. The IntelliCage was controlled by a computer with dedicated software (IntelliCagePlus), executing preprogrammed experimental schedules and registering the number and duration of visits to the corner chambers, nose-pokes to the door openings and lickings as behavioural measures for each mouse. To randomize treatment groups and allow non-competitive access to the corners mice were housed in 4 Intellicages in balanced groups of the same sex (e.g. 4 control + 4 caspase). The mice were group-housed in these groups from weaning (cage type Tecniplast Green Line GR900), at least 10 weeks before the start of Intellicage experiments. All tests in Intellicage system were done in the order they are listed below on the consecutive days without taking mice out from the cages except as on two cleaning days.

Free adaptation. In the beginning of the test, the mice were released in the IntelliCage during the light phase at 9 am with all doors open allowing unlimited access to the water bottles (free adaptation). Animals were allowed to explore the new environment for 3 consecutive days. Exploratory, locomotor and circadian activity were measured as a number of corner visits or as nose-pokes to the water bottles per hour for each day separately (day 1 – adaptation phase, day 2 and 3 – basic activity). Similarly, drinking behaviour was measured as a number of licks/h.

Adaptation to nose-poke. On the fourth day, all doors were closed at the beginning of the experiment and mice were required to poke into closed gates to reach drinking tubes. Only the first nose-poke of the visit opened the door for 5 seconds (pre-defined time). Animals had to start a new visit in order to get access to water again. This rule was the same in all experiments requiring nose-poking.

Saccharin preference. In this task, all four corners operated the same way, 24 h per day: doors opened spontaneously for a 7-s drinking period on the entry to corner. Each corner contained a bottle of saccharine on one side and a bottle of

bioRxiv preprint doi: https://doi.org/10.1101/2023.01.06.522982; this version posted January 6, 2023. The copyright holder for this preprint (which was not certified by peer review) is the author/funder, who has granted bioRxiv a license to display the preprint in perpetuity. It is made available under aCC-BY-ND 4.0 International license.

water on the other. High and low saccharine concentrations were chosen based on the previous research (Pijlman et al., 2003; Sclafani et al., 2010). Every day, saccharine and water sides were alternated to exclude side preference. During the first three days, mice were suggested to choose between two low saccharine concentrations 0.01% (S1) and 0.03% (S2) assigned to two opposite corners each. During the next three days the lowest 0.01% (S1) concentration was exchanged to the highest 0.3% (S3) one and the order of the corners was changed as well. For better understanding of the schedule, below there is a simplified scheme with the corners and sides assignments.

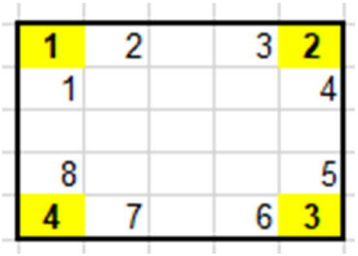

Day 1	S-Pref 1	S1 - 2,5; S2 - 4,7; W - 1,3,6,8
Day 2	S-Pref 1	S1 - 1,6; S2 - 3,8; W - 2,4,5,7
Day 3	S-Pref 1	S1 - 2,5; S2 - 4,7; W - 1,3,6,8
Day 1	S-Pref 2	S2 - 4,7; S3 - 2,5; W - 1,3,6,8
Day 2	S-Pref 2	S2 - 3,8; S3 - 1,6; W - 2,4,5,7
Day 3	S-Pref 2	S2 - 4,7; S3 - 2,5; W - 1,3,6,8

The preference score was calculated as percentage of the number of licks to the certain liquid (two saccharine liquids of different concentrations and two water liquids in corresponding saccharine corners) from the total number of licks during the last two days of each session.

Delay discounting. In this experiment all four corners were accessible to all animals and contained 0.3% saccharine liquid (S3) on one side of the corner and water on the other side. The order of the bottles was as follows (see the picture above): S3 - 1,3,6,8; W - 2,4,5,7. On Day 0 both doors to the water and saccharine opened simultaneously for 7 s upon the entry to the corner. On Day 1, saccharine door opened with a 0.5-s delay, while the water bottle door opened immediately. Next day, delay before the opening of the saccharine door increased to 1 s and then for 1 s every next 24 h. After 4 days, this resulted in a delay of 5 s. A saccharin

bioRxiv preprint doi: https://doi.org/10.1101/2023.01.06.522982; this version posted January 6, 2023. The copyright holder for this preprint (which was not certified by peer review) is the author/funder, who has granted bioRxiv a license to display the preprint in perpetuity. It is made available under aCC-BY-ND 4.0 International license.

preference score was calculated as percentage of lick number to saccharin bottles form a total lick number (saccharin + water).

Saccharine extinction and avoidance. In these two tasks the set up was very similar in general and differed only in the third phase. Water was always available on the entry in two corners for all animals. Saccharine 0.3% (S3) was available with a rule in one corner for 4 specific mice (2 caspase+2 controls) and in another corner for the remaining 4 mice to avoid competition. The rule was as follows: to get the saccharine mice had to nose-poke in one of the side doors, it triggered the LED light above this door for 1.5 s and then it opened after an extra 0.5-s delay for 5 s. Mice had to repeat the sequence in order to get the additional access to the saccharine. In Phase 1 (33 h), mice were learning the rule; in Phase 2 (48 h) mice were adapted to the rule and the basic activity was measured; in Phase 3 (38 h) saccharine bottles were emptied for the “Extinction” experiment. In the “Avoidance” experiment mice went through the same sequence of events, but in the Phase 1 saccharine bottles were back, and the order of the corners was changed, so they had to learn new rules (re-learning). In Phase 3 (Avoidance), mice received 0.2-bar air puffs in the saccharine door with 25% probability. Activity was measured during the whole experiment as a number of nose-pokes/h. Similarly, drinking behaviour was measured as licks/h.

Fear conditioning (FC). For these experiments, the same “Intellicage cohort” of mice was used. Animals were single-housed after the Intellicage experiments and given 2 weeks of adaptation prior the FC. The FC protocol was based on previously published studies (Mennesson et al., 2020) with few modifications and consisted from three phases: acquisition, context test and cue test. Shortly, mice were placed one by one to the test chamber (Video fear conditioning, Med Associates Inc.) for the fear *acquisition and conditioning*. After 120-s of free exploration, a 30-s 5 kHz 90-dB cue tone sounded from the wall-mounted speakers, co-terminated with a 2-s

bioRxiv preprint doi: https://doi.org/10.1101/2023.01.06.522982; this version posted January 6, 2023. The copyright holder for this preprint (which was not certified by peer review) is the author/funder, who has granted bioRxiv a license to display the preprint in perpetuity. It is made available under aCC-BY-ND 4.0 International license.

scrambled 0.6-mA shock through the grid floor. Cue-shock pairs were repeated twice again with 90 and 60 s inter-trial intervals, after that the session was finished with 120 s of free exploration. Chamber light, near-infrared light and a fan were on during all phases. After each mouse the chamber was cleaned with water.

Nine days later, the mice were tested in the same chambers for the *context*-induced retrieval of the fear memory. For that, the mouse was placed to the same testing chamber with identical conditions as before, except for no cue tones or shocks, for 300 s of free exploration.

Five hours after the context test, *cue*-induced retrieval of the fear memory was assessed in the conditioning chamber with the floor and wall material and the shape of the chamber changed to exclude the context component. After 120 s of free exploration, the mouse was introduced with twenty 30-s cue tones (identical with those used during conditioning) separated by 5-s inter-tone intervals. After each mouse, the chamber was cleaned with 70% ethanol.

Freezing time and number of freezing episodes were automatically analyzed by Video Freeze Software (Med Associates Inc.) separately for each component of the test phases.

Drugs: Morphine hydrochloride (University Pharmacy, Helsinki, Finland) was dissolved in physiological saline (0.9% NaCl) on the day of treatment. Morphine was injected in a volume of 10 mL/kg body weight.

Statistics. For behavioural experiments, statistical analysis was done using SPSS (IBM SPSS Statistics, 28.0.0.0) while graphs were drawn with Prism 8.1.10. The data were tested for normality and homogeneity of variance using the Kolmogorov-Smirnov and Levene's tests, respectively. Statistical analyses of the data were done using one-way, univariate and repeated measures two-way ANOVAs unless stated otherwise. In case of significant main effect or interaction, post-hoc tests were

bioRxiv preprint doi: https://doi.org/10.1101/2023.01.06.522982; this version posted January 6, 2023. The copyright holder for this preprint (which was not certified by peer review) is the author/funder, who has granted bioRxiv a license to display the preprint in perpetuity. It is made available under aCC-BY-ND 4.0 International license.

performed using multiple comparisons test with Bonferroni correction. The level of significance was set at 0.05. All data are shown as means ± SEM.

Reference list

Björklund A, Dunnett SB. 2007. Dopamine neuron systems in the brain: an update. *Trends Neurosci* 30:194–202. doi:10.1016/j.tins.2007.03.006

Bouarab C, Thompson B, Polter AM. 2019. VTA GABA Neurons at the Interface of Stress and Reward. *Front Neural Circuits* 13:1–12. doi:10.3389/fncir.2019.00078

Broussot L, Contesse T, Costa-Campos R, Glangetas C, Royon L, Fofo H, Lorivel T, Georges F, Fernandez SP, Barik J. 2022. A non-canonical GABAergic pathway to the VTA promotes unconditioned freezing. *Mol Psychiatry* 1–13. doi:10.1038/s41380-022-01765-7

Cadwell CR, Scala F, Li S, Livrizzi G, Shen S, Sandberg R, Jiang X, Tolias AS. 2017. Multimodal profiling of single-cell morphology, electrophysiology, and gene expression using Patch-seq. *Nat Protoc* 12:2531–2553. doi:10.1038/nprot.2017.120

Cai J, Tong Q. 2022. Anatomy and Function of Ventral Tegmental Area Glutamate Neurons. *Front Neural Circuits* 16. doi:10.3389/fncir.2022.867053

Concetti C, Bracey EF, Peleg-Raibstein D, Burdakov D. 2020. Control of fear extinction by hypothalamic melanin-concentrating hormone–expressing neurons. *Proc Natl Acad Sci U S A* 117:22514–22521. doi:10.1073/pnas.2007993117

Corre J, van Zessen R, Loureiro M, Patriarchi T, Tian L, Pascoli V, Lüscher C. 2018. Dopamine neurons projecting to medial shell of the nucleus accumbens drive

bioRxiv preprint doi: https://doi.org/10.1101/2023.01.06.522982; this version posted January 6, 2023. The copyright holder for this preprint (which was not certified by peer review) is the author/funder, who has granted bioRxiv a license to display the preprint in perpetuity. It is made available under aCC-BY-ND 4.0 International license.

heroin reinforcement. *Elife* 7:1–22. doi:10.7554/eLife.39945

Cover KK, Maeng LY, Lebrón-Milad K, Milad MR. 2014. Mechanisms of estradiol in fear circuitry: Implications for sex differences in psychopathology. *Transl Psychiatry* 4. doi:10.1038/tp.2014.67

Dobi A, Margolis EB, Wang HL, Harvey BK, Morales M. 2010. Glutamatergic and nonglutamatergic neurons of the ventral tegmental area establish local synaptic contacts with dopaminergic and nondopaminergic neurons. *J Neurosci* 30:218–229. doi:10.1523/JNEUROSCI.3884-09.2010

Elsilä L V., Harkki J, Enberg E, Martti A, Linden AM, Korpi ER. 2022. Effects of acute lysergic acid diethylamide on intermittent ethanol and sucrose drinking and intracranial self-stimulation in C57BL/6 mice. *J Psychopharmacol* 36:860–874. doi:10.1177/02698811221104641

Franklin KBJ, Paxinos G. 2007. The Mouse Brain in Stereotaxic Coordinates (map), Academic Press.

Fuzik J, Zeisel A, Máté Z, Calvigioni D, Yanagawa Y, Szabó G, Linnarsson S, Harkany T. 2016. Integration of electrophysiological recordings with single-cell RNA-seq data identifies neuronal subtypes. *Nat Biotechnol* 34:175–183. doi:10.1038/nbt.3443

Gao C, Leng Y, Ma J, Rooke V, Rodriguez-Gonzalez S, Ramakrishnan C, Deisseroth K, Penzo MA. 2020. Two genetically, anatomically and functionally distinct cell types segregate across anteroposterior axis of paraventricular thalamus. *Nat Neurosci* 23:217–228. doi:10.1038/s41593-019-0572-3

Gomes-de-Souza L, Costa-Ferreira W, Mendonça MM, Xavier CH, Crestani CC. 2021. Lateral hypothalamus involvement in control of stress response by bed nucleus of the stria terminalis endocannabinoid neurotransmission in male rats. *Sci Rep*

bioRxiv preprint doi: https://doi.org/10.1101/2023.01.06.522982; this version posted January 6, 2023. The copyright holder for this preprint (which was not certified by peer review) is the author/funder, who has granted bioRxiv a license to display the preprint in perpetuity. It is made available under aCC-BY-ND 4.0 International license.

11:1–12. doi:10.1038/s41598-021-95401-z

Goode TD, Maren S. 2017. Role of the bed nucleus of the stria terminalis in aversive learning and memory. *Learn Mem* 24:480–491. doi:10.1101/lm.044206.116

Hnasko TS, Hjelmstad GO, Fields HL, Edwards RH. 2012. Ventral Tegmental Area Glutamate Neurons: Electrophysiological Properties and Projections. *J Neurosci* 32:15076–15085. doi:10.1523/JNEUROSCI.3128-12.2012

Jalabert M, Bourdy R, Courtin J, Veinante P, Manzoni OJ, Barrot M, Georges F. 2011. Neuronal circuits underlying acute morphine action on dopamine neurons. *Proc Natl Acad Sci U S A* 108:16446–16450. doi:10.1073/pnas.1105418108

Johnson SW, North RA. 1992. Opioids excite dopamine neurons by hyperpolarization of local interneurons. *J Neurosci* 12:483–488.

Kalivas PW, Richardson-Carlson R, Van Orden G. 1986. Cross-sensitization between foot shock stress and enkephalin-induced motor activity. *Biol Psychiatry* 21:939–950. doi:10.1016/0006-3223(86)90268-4

Keifer OP, Hurt RC, Ressler KJ, Marvar PJ. 2015. The physiology of fear: Reconceptualizing the role of the central amygdala in fear learning. *Physiology* 30:389–401. doi:10.1152/physiol.00058.2014

Kim Y, Yang GR, Pradhan K, Venkataraju KU, Bota M, García del Molino LC, Fitzgerald G, Ram K, He M, Levine JM, Mitra P, Huang ZJ, Wang X-J, Osten P. 2017. Brain-wide Maps Reveal Stereotyped Cell-Type-Based Cortical Architecture and Subcortical Sexual Dimorphism. *Cell* 171:456-469.e22. doi:10.1016/j.cell.2017.09.020

Kirouac GJ. 2021. The Paraventricular Nucleus of the Thalamus as an Integrating and Relay Node in the Brain Anxiety Network. *Front Behav Neurosci* 15:1–14. doi:10.3389/fnbeh.2021.627633

bioRxiv preprint doi: https://doi.org/10.1101/2023.01.06.522982; this version posted January 6, 2023. The copyright holder for this preprint (which was not certified by peer review) is the author/funder, who has granted bioRxiv a license to display the preprint in perpetuity. It is made available under aCC-BY-ND 4.0 International license.

Kirouac GJ. 2015. Placing the paraventricular nucleus of the thalamus within the brain circuits that control behaviour. *Neurosci Biobehav Rev* 56:315–329. doi:10.1016/j.neubiorev.2015.08.005

Koob GF, Arends MA, Le Moal M. 2014a. Drugs, Addiction, and the Brain - Alcohol, Drugs, Addiction, and the Brain. doi:10.1016/B978-0-12-386937-1.00006-4

Koob GF, Arends MA, Le Moal M. 2014b. Opioids, Drugs, Addiction, and the Brain. doi:10.1016/B978-0-12-386937-1.00005-2

Kuzmin A, Semenova S, Zvartau EE, Van Ree JM. 1996. Enhancement of morphine self-administration in drug naive, inbred strains of mice by acute emotional stress. *Eur Neuropsychopharmacol* 6:63–68. doi:10.1016/0924-977X(95)00066-X

Lainiola M, Hietala L, Linden AM, Aitta-aho T. 2019. The lack of conditioned place preference, but unaltered stimulatory and ataxic effects of alcohol in mGluR3-KO mice. *J Psychopharmacol* 33:855–864. doi:10.1177/0269881119844178

Lebow MA, Chen A. 2016. Overshadowed by the amygdala: the bed nucleus of the stria terminalis emerges as key to psychiatric disorders. *Mol Psychiatry* 21:450–463. doi:10.1038/mp.2016.1

Leyton M, Stewart J. 1990. Preexposure to foot-shock sensitizes the locomotor response to subsequent systemic morphine and intra-nucleus accumbens amphetamine. *Pharmacol Biochem Behav* 37:303–310. doi:10.1016/0091-3057(90)90339-J

Li X, Qi J, Yamaguchi T, Wang HL, Morales M. 2013. Heterogeneous composition of dopamine neurons of the rat A10 region: Molecular evidence for diverse signaling properties. *Brain Struct Funct* 218:1159–1176. doi:10.1007/s00429-012-0452-z

Li Y, Li CY, Xi W, Jin S, Wu ZH, Jiang P, Dong P, He X Bin, Xu FQ, Duan S, Zhou YD, Li

bioRxiv preprint doi: https://doi.org/10.1101/2023.01.06.522982; this version posted January 6, 2023. The copyright holder for this preprint (which was not certified by peer review) is the author/funder, who has granted bioRxiv a license to display the preprint in perpetuity. It is made available under aCC-BY-ND 4.0 International license.

XM. 2019. Rostral and Caudal Ventral Tegmental Area GABAergic Inputs to Different Dorsal Raphe Neurons Participate in Opioid Dependence. *Neuron* 101:748-761.e5. doi:10.1016/j.neuron.2018.12.012

López-Ferreras L, Richard JE, Anderberg RH, Nilsson FH, Olandersson K, Kanoski SE, Skibicka KP. 2017. Ghrelin's control of food reward and body weight in the lateral hypothalamic area is sexually dimorphic. *Physiol Behav* 176:40–49. doi:10.1016/j.physbeh.2017.02.011

Maren S. 2001. Neurobiology of Pavlovian Fear Conditioning. *Annu Rev Neurosci* 24:897–931. doi:10.1146/annurev.neuro.24.1.897

Martin WR, Wikler A, Eades CG, Pescor FT. 1963. Tolerance to and physical dependence on morphine in rats. *Psychopharmacologia* 4:247–260. doi:10.1007/BF00408180

Mennesson M, Orav E, Gigliotta A, Kulesskaya N, Saarnio S, Kirjavainen A, Kesaf S, Winkel F, Pou ML, Umemori J, Voikar V, Risbrough V, Partanen J, Castrén E, Lauri SE, Hovatta I. 2020. Kainate receptor auxiliary subunit neto2-related cued fear conditioning impairments associate with defects in amygdala development and excitability. *eNeuro* 7:1–15. doi:10.1523/ENEURO.0541-19.2020

Mitchell SH. 2014. Assessing delay discounting in mice. *Curr Protoc Neurosci* 1–15. doi:10.1002/0471142301.ns0830s66

Nagaeva E, Zubarev I, Bengtsson Gonzales C, Forss M, Nikouei K, de Miguel E, Elsilä L, Linden A-M, Hjerling-Leffler J, Augustine GJ, Korpi ER. 2020. Heterogeneous somatostatin-expressing neuron population in mouse ventral tegmental area. *Elife* 9:1–29. doi:10.7554/eLife.59328

Nagaeva E, Zubarev I, Korpi E. 2021. Electrophysiological Properties of Neurons: Current-Clamp Recordings in Mouse Brain Slices and Firing-Pattern Analysis.

bioRxiv preprint doi: https://doi.org/10.1101/2023.01.06.522982; this version posted January 6, 2023. The copyright holder for this preprint (which was not certified by peer review) is the author/funder, who has granted bioRxiv a license to display the preprint in perpetuity. It is made available under aCC-BY-ND 4.0 International license.

BIO-PROTOCOL 11:1–23. doi:10.21769/BioProtoc.4061

Nugent FS, Penick EC, Kauer JA. 2007. Opioids block long-term potentiation of inhibitory synapses. *Nature* 446:1086–1090. doi:10.1038/nature05726

Penzo MA, Robert V, Tucciarone J, De Bundel D, Wang M, Van Aelst L, Darvas M, Parada LF, Palmiter RD, He M, Huang ZJ, Li B. 2015. The paraventricular thalamus controls a central amygdala fear circuit. *Nature* 519:455–459. doi:10.1038/nature13978

Pernold K, Iannello F, Low BE, Rigamonti M, Rosati G, Scavizzi F, Wang J, Raspa M, Wiles M V., Ulfhake B. 2019. Towards large scale automated cage monitoring - Diurnal rhythm and impact of interventions on in-cage activity of C57BL/6J mice recorded 24/7 with a non-disrupting capacitive-based technique. *PLoS One* 14:1–20. doi:10.1371/journal.pone.0211063

Pernold K, Rullman E, Ulfhake B. 2021. Major oscillations in spontaneous home-cage activity in C57BL/6 mice housed under constant conditions. *Sci Rep* 11:1–13. doi:10.1038/s41598-021-84141-9

Phillips RA, Tuscher JJ, Black SL, Andraka E, Fitzgerald ND, Ianov L, Day JJ. 2022. An atlas of transcriptionally defined cell populations in the rat ventral tegmental area. *Cell Rep* 39:110616. doi:10.1016/j.celrep.2022.110616

Pijlman FTA, Wolterink G, Van Ree JM. 2003. Physical and emotional stress have differential effects on preference for saccharine and open field behaviour in rats. *Behav Brain Res* 139:131–138. doi:10.1016/S0166-4328(02)00124-9

Procaccini C, Aitta-Aho T, Jaako-Movits K, Zharkovsky A, Panhelainen A, Sprengel R, Linden AM, Korpi ER. 2011. Excessive novelty-induced c-Fos expression and altered neurogenesis in the hippocampus of GluA1 knockout mice. *Eur J Neurosci* 33:161–174. doi:10.1111/j.1460-9568.2010.07485.x

bioRxiv preprint doi: https://doi.org/10.1101/2023.01.06.522982; this version posted January 6, 2023. The copyright holder for this preprint (which was not certified by peer review) is the author/funder, who has granted bioRxiv a license to display the preprint in perpetuity. It is made available under aCC-BY-ND 4.0 International license.

Quina LA, Walker A, Morton G, Han V, Turner EE. 2020. GAD2 expression defines a class of excitatory lateral habenula neurons in mice that project to the raphe and pontine tegmentum. *eNeuro* 7:1–19. doi:10.1523/ENEURO.0527-19.2020

R.G. L. 1987. The use of a plus-maze to measure anxiety in the mouse. *Psychopharmacology (Berl)* 92:180–185.

Radwanska K, Kaczmarek L. 2012. Characterization of an alcohol addiction-prone phenotype in mice. *Addict Biol* 17:601–612. doi:10.1111/j.1369-1600.2011.00394.x

Schultz W, Dayan P, Montague PR. 1997. A neural substrate of prediction and reward. *Science (80-)*. doi:10.1126/science.275.5306.1593

Sclafani A. 2006. Enhanced sucrose and Polycose preference in sweet “sensitive” (C57BL/6J) and “subsensitive” (129P3/J) mice after experience with these saccharides. *Physiol Behav* 87:745–756. doi:10.1016/j.physbeh.2006.01.016

Sclafani A, Bahrani M, Zukerman S, Ackroff K. 2010. Stevia and saccharin preferences in rats and mice. *Chem Senses* 35:433–443. doi:10.1093/chemse/bjq033

Shackman AJ, Fox AS. 2016. Contributions of the central extended amygdala to fear and anxiety. *J Neurosci* 36:8050–8063. doi:10.1523/JNEUROSCI.0982-16.2016

Shaham Y, Alvares K, Nespor SM, Grunberg NE. 1992. Effect of stress on oral morphine and fentanyl self-administration in rats. *Pharmacol Biochem Behav* 41:615–619. doi:10.1016/0091-3057(92)90382-P

Stamatakis AM, Jennings JH, Ung RL, Blair GA, Weinberg RJ, Neve RL, Boyce F, Mattis J, Ramakrishnan C, Deisseroth K, Stuber GD. 2013. A Unique Population of Ventral Tegmental Area Neurons Inhibits the Lateral Habenula to Promote Reward. *Neuron* 80:1039–1053. doi:10.1016/j.neuron.2013.08.023

bioRxiv preprint doi: https://doi.org/10.1101/2023.01.06.522982; this version posted January 6, 2023. The copyright holder for this preprint (which was not certified by peer review) is the author/funder, who has granted bioRxiv a license to display the preprint in perpetuity. It is made available under aCC-BY-ND 4.0 International license.

Sucher NJ, Deitcher DL. 1995. PCR and patch-clamp analysis of single neurons. *Neuron* 14:1095–1100. doi:10.1016/0896-6273(95)90257-0

Tan KR, Yvon C, Turiault M, Mirzabekov JJ, Doehner J, Labouèbe G, Deisseroth K, Tye KM, Lüscher C. 2012. GABA Neurons of the VTA Drive Conditioned Place Aversion. *Neuron* 73:1173–1183. doi:10.1016/j.neuron.2012.02.015

Taylor SR, Badurek S, Dileone RJ, Nashmi R, Minichiello L, Picciotto MR. 2014. GABAergic and glutamatergic efferents of the mouse ventral tegmental area. *J Comp Neurol* 522:3308–3334. doi:10.1002/cne.23603

Uchida K, Otsuka H, Morishita M, Tsukahara S, Sato T, Sakimura K, Itoi K. 2019. Correction to: Female-biased sexual dimorphism of corticotropin-releasing factor neurons in the bed nucleus of the stria terminalis (Biology of Sex Differences (2019) 10 (6) DOI: 10.1186/s13293-019-0221-2). *Biol Sex Differ* 10:1–11. doi:10.1186/s13293-019-0224-z

Van Zessen R, Phillips JL, Budygin EA, Stuber GD. 2012. Activation of VTA GABA Neurons Disrupts Reward Consumption. *Neuron* 73:1184–1194. doi:10.1016/j.neuron.2012.02.016

Vashchinkina E, Panhelainen A, Vekovischeva OY, Aitta-Aho T, Ebert B, Ator NA, Korpi ER. 2012. GABA site agonist gaboxadol induces addiction-predicting persistent changes in ventral tegmental area dopamine neurons but is not rewarding in mice or baboons. *J Neurosci* 32:5310–5320. doi:10.1523/JNEUROSCI.4697-11.2012

Viollet C, Lepousez G, Loudes C, Videau C, Simon A, Epelbaum J. 2008. Somatostatinergic systems in brain: Networks and functions. *Mol Cell Endocrinol* 286:75–87. doi:10.1016/j.mce.2007.09.007

Viollet C, Simon A, Tolle V, Labarthe A, Grouselle D, Loe-Mie Y, Simonneau M, Martel

bioRxiv preprint doi: https://doi.org/10.1101/2023.01.06.522982; this version posted January 6, 2023. The copyright holder for this preprint (which was not certified by peer review) is the author/funder, who has granted bioRxiv a license to display the preprint in perpetuity. It is made available under aCC-BY-ND 4.0 International license.

G, Epelbaum J. 2017. Somatostatin-IRES-cre mice: Between knockout and wild-type? *Front Endocrinol (Lausanne)* 8:1–8. doi:10.3389/fendo.2017.00131

Yamaguchi T, Qi J, Wang HL, Zhang S, Morales M. 2015. Glutamatergic and dopaminergic neurons in the mouse ventral tegmental area. *Eur J Neurosci* 41:760–772. doi:10.1111/ejn.12818

Yamaguchi T, Wang H-L, Li X, Ng TH, Morales M. 2011. Mesocorticolimbic Glutamatergic Pathway. *J Neurosci* 31:8476–8490. doi:10.1523/JNEUROSCI.1598-11.2011

Yu X, Li W, Ma Y, Tossell K, Harris JJ, Harding EC, Ba W, Miracca G, Wang D, Li L, Guo J, Chen M, Li Y, Yustos R, Vyssotski AL, Burdakov D, Yang Q, Dong H, Franks NP, Wisden W. 2019. GABA and glutamate neurons in the VTA regulate sleep and wakefulness. *Nat Neurosci* 22:106–119. doi:10.1038/s41593-018-0288-9

Yu X, Zhao G, Wang D, Wang S, Li R, Li A, Wang H, Nollet M, Chun YY, Zhao T, Yustos R, Li H, Zhao J, Li J, Cai M, Vyssotski AL, Li Y, Dong H, Franks NP, Wisden W. 2022. A specific circuit in the midbrain detects stress and induces restorative sleep. *Science (80-)* 377:63–72. doi:10.1126/science.abn0853

Zell V, Steinkellner T, Hollon NG, Warlow SM, Souter E, Faget L, Hunker AC, Jin X, Zweifel LS, Hnasko TS. 2020. VTA Glutamate Neuron Activity Drives Positive Reinforcement Absent Dopamine Co-release. *Neuron* 107:864-873.e4. doi:10.1016/j.neuron.2020.06.011

bioRxiv preprint doi: https://doi.org/10.1101/2023.01.06.522982; this version posted January 6, 2023. The copyright holder for this preprint (which was not certified by peer review) is the author/funder, who has granted bioRxiv a license to display the preprint in perpetuity. It is made available under aCC-BY-ND 4.0 International license.

Acknowledgements

The following core facilities were essential for the project: Biomedicum Imaging Unit of the University of Helsinki; Mouse Behavioural Phenotyping Facility of the University of Helsinki, supported by Helsinki Institute of Life Science and Biocenter, Finland; Biostatistics Consulting Service of the University of Helsinki; Canadian Neurophotonics Platform, Québec, Canada. The authors are grateful for the expert technical assistance and fruitful discussion by Heidi Hytönen, Vootele Voikar, Ivan Zubarev, Merja Voutilainen, Mikko Airavaara, Lauren van den Broecke and Laura Martikainen.

Funding

The project was supported by the Academy of Finland (1317399; 330298), the Sigrid Juselius Foundation, Otto Malm Foundation and Biomedicum Helsinki Foundation. The funders had no role in study design, data collection and interpretation, or the decision to submit the work for publication.

Author contributions

E.N., A.S., A.M.L. and E.R.K. planned the project. E.N. performed electrophysiology, single-cell qPCR, immunohistochemistry (IHC) and imaging for the tracing experiments, Intellicage and fear-conditioning (FC) data analysis. A.S. and L.V.E. performed intracranial injections, IHC and imaging for caspase and tracing experiments. A.S. performed and analyzed all behavioural experiments for caspase animal cohorts 1 and 2. A.M.L. planned the breeding of experimental animals and performed FC experiments. M.R. performed intracranial injections to CeM. J.U. consulted on the qPCR experiments and data analysis. K.E. performed imaging and cell counting for caspase experiments. E.N. wrote the first draft of the full

bioRxiv preprint doi: https://doi.org/10.1101/2023.01.06.522982; this version posted January 6, 2023. The copyright holder for this preprint (which was not certified by peer review) is the author/funder, who has granted bioRxiv a license to display the preprint in perpetuity. It is made available under aCC-BY-ND 4.0 International license.

manuscript, all other authors approved the manuscript, with E.N., A.S, A.M.L. and E.R.K. writing the final version.

The authors declare no competing interests.

bioRxiv preprint doi: https://doi.org/10.1101/2023.01.06.522982; this version posted January 6, 2023. The copyright holder for this preprint (which was not certified by peer review) is the author/funder, who has granted bioRxiv a license to display the preprint in perpetuity. It is made available under aCC-BY-ND 4.0 International license.

Supplementary Figures

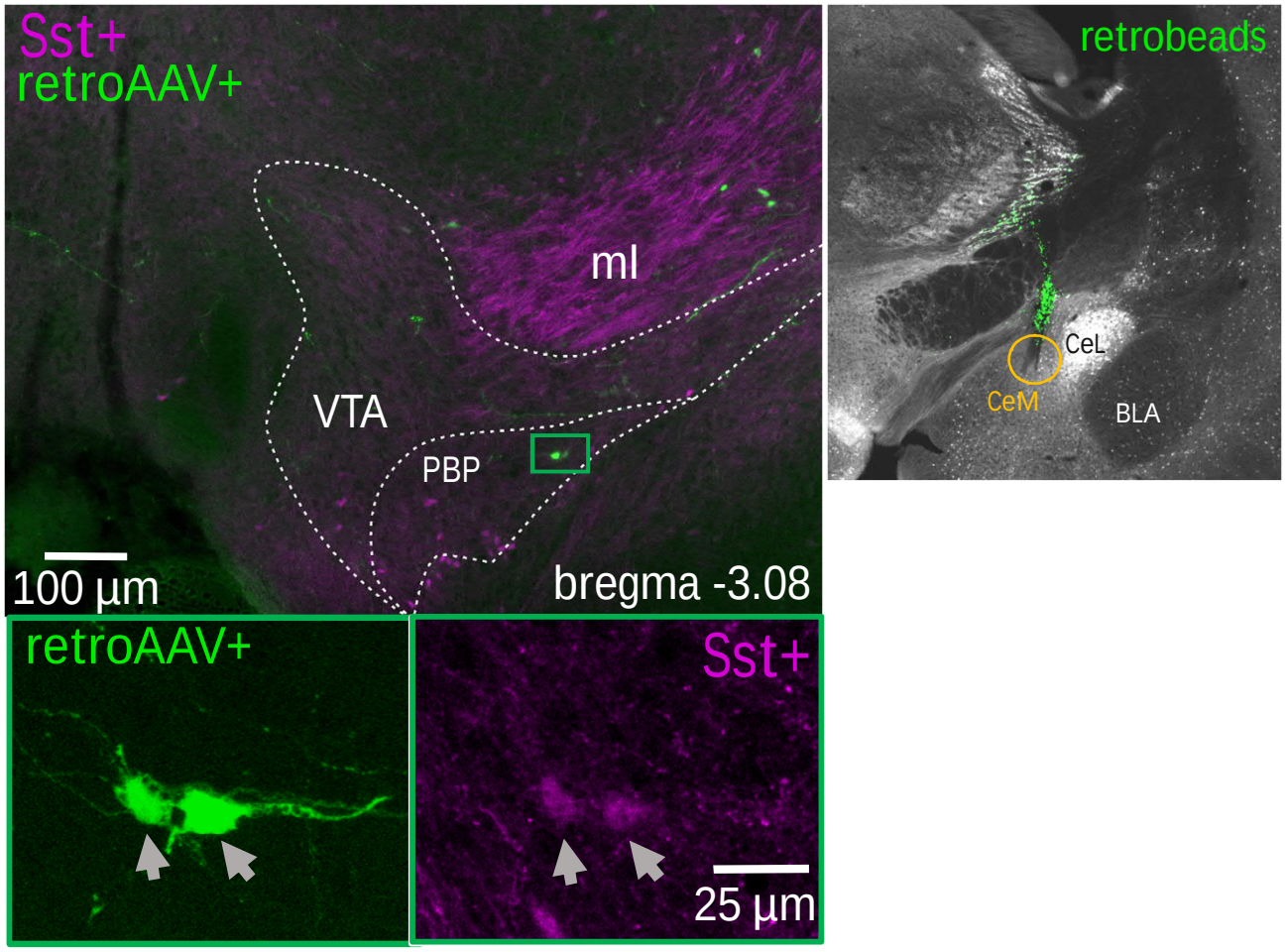

Figure S1. Backtracing from the medial part of the Central Amygdala. Examples of the backtraced neurons in the VTA at the bregma level -3.08 mm in Sst-tdTomato (magenta) mouse. The image on the right shows retrobeads in the injection site (CeM). The yellow circle shows the actual unilateral injection spot. On the top left, the green rectangle shows ipsilaterally traced neurons. The lower panels are the magnified images of the green rectangle. *BLA* – basolateral amygdala; *CeL* – lateral part of the central amygdala; *CeM* – medial part of the central amygdala; *ml* – medial lemniscus; *PBP* – parabrachial pigmented nucleus of the VTA; *VTA* – ventral tegmental area.

bioRxiv preprint doi: https://doi.org/10.1101/2023.01.06.522982; this version posted January 6, 2023. The copyright holder for this preprint (which was not certified by peer review) is the author/funder, who has granted bioRxiv a license to display the preprint in perpetuity. It is made available under aCC-BY-ND 4.0 International license.

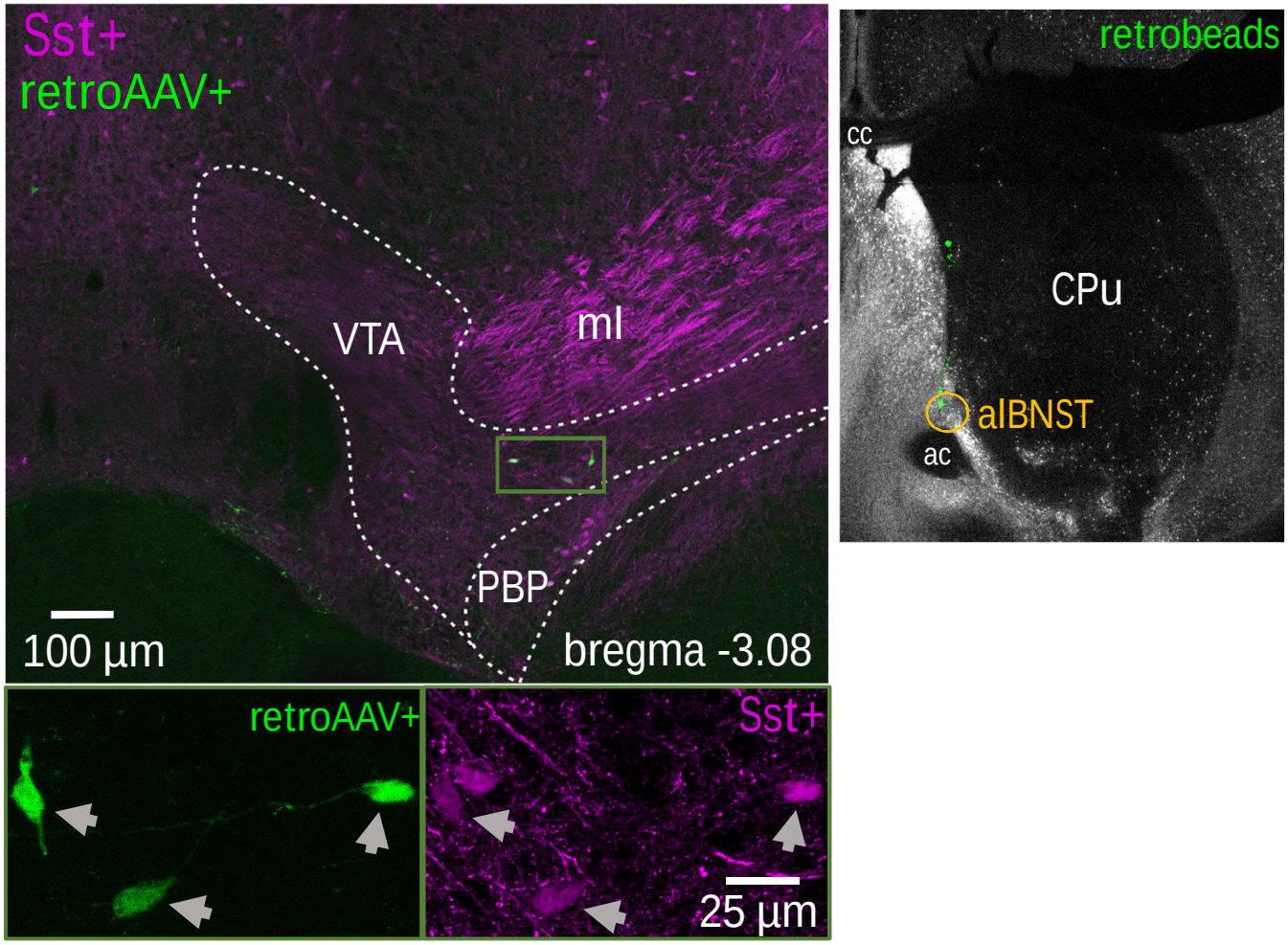

Figure S2. Backtracing from the anterolateral part of the Bed Nucleus of Stria Terminalis. Examples of the backtraced neurons in the VTA at the bregma level -3.08 mm in Sst-tdTomato (magenta) mouse. The image on the right shows retrobeads in the injection site (alBNST). The yellow circle shows the actual injection spot. On the top left, the green rectangle shows ipsilaterally traced neurons. Lower panels are magnified images inside green rectangle split by fluorescent channels. *ac* – anterior commissure; *alBNST* – bed nucleus of the stria terminalis, antero-lateral part; *cc* – corpus callosum; *CPu*- caudatus-putamen (striatum); *ml* – medial lemniscus; *PBP* – parabrachial pigmented nucleus of the VTA; *VTA* – ventral tegmental area.

bioRxiv preprint doi: https://doi.org/10.1101/2023.01.06.522982; this version posted January 6, 2023. The copyright holder for this preprint (which was not certified by peer review) is the author/funder, who has granted bioRxiv a license to display the preprint in perpetuity. It is made available under aCC-BY-ND 4.0 International license.

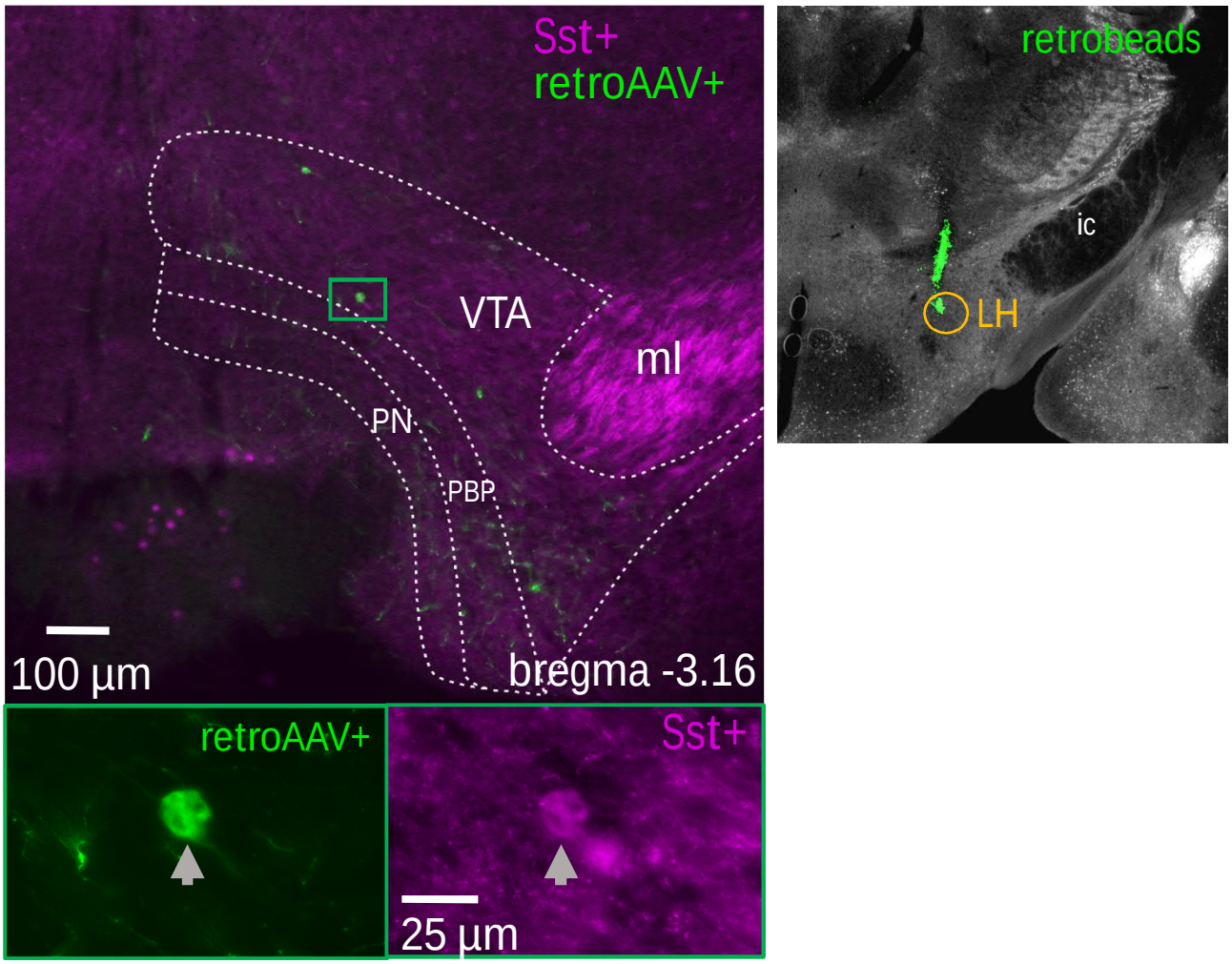

Figure S3. Backtracing from the Lateral Hypothalamus. Examples of the backtraced neurons in the VTA at the bregma level -3.28 mm in Sst-tdTomato (magenta) mouse. The right upper corner shows retrobeads at the injection site (LH). The yellow circle shows the actual unilateral injection spot. On the top left, the green rectangle shows an ipsilaterally traced neuron. Lower panels are magnified images inside the green rectangle split by fluorescent channels. *ic* – internal capsule; *LH* – lateral hypothalamus; *ml* – medial lemniscus; *PBP* – parabrachial pigmented nucleus of the VTA; *PN* – paranigral nucleus of VTA; *VTA* – ventral tegmental area.

bioRxiv preprint doi: https://doi.org/10.1101/2023.01.06.522982; this version posted January 6, 2023. The copyright holder for this preprint (which was not certified by peer review) is the author/funder, who has granted bioRxiv a license to display the preprint in perpetuity. It is made available under aCC-BY-ND 4.0 International license.

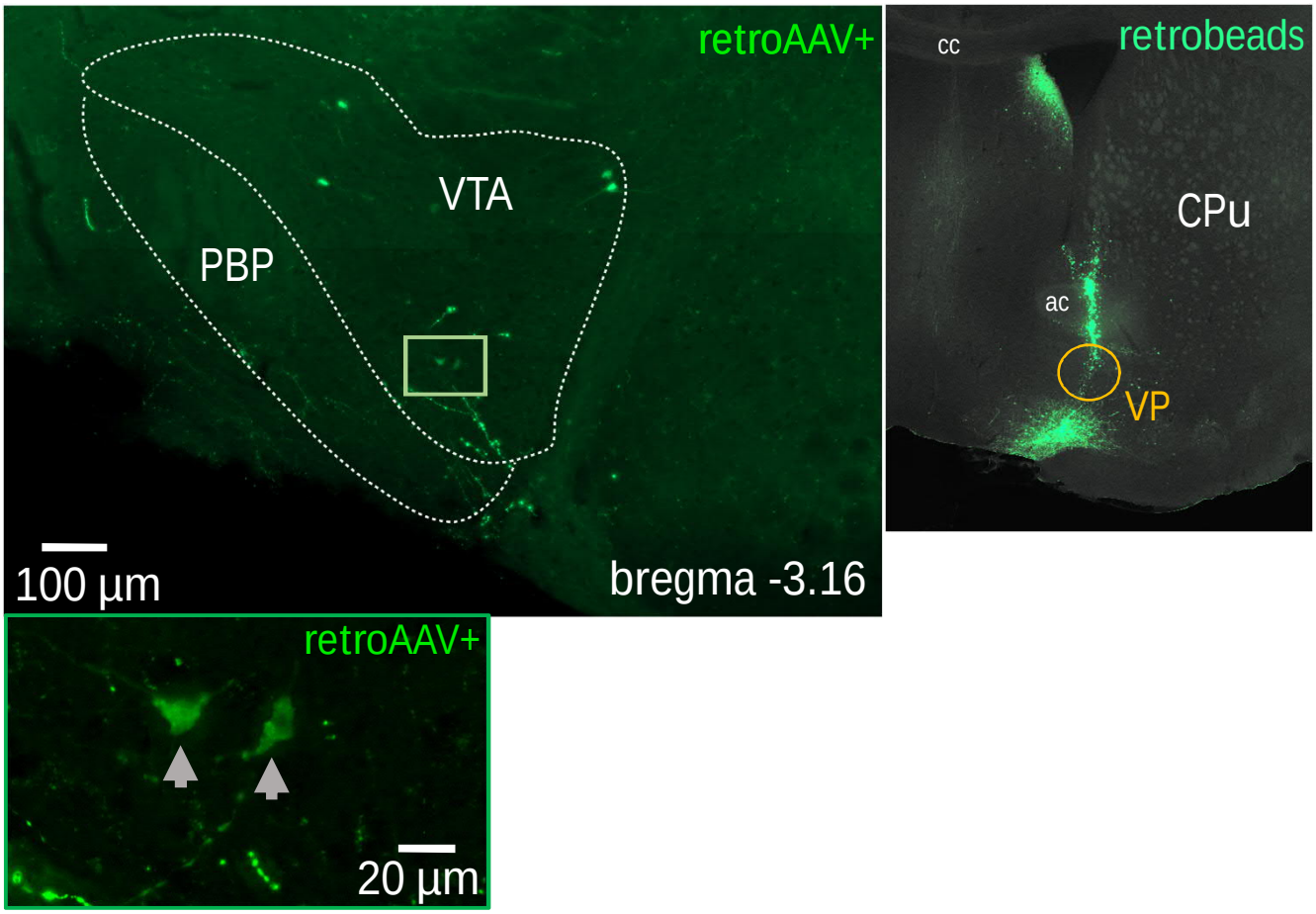

Figure S4. Backtracing from the Ventral Pallidum. Examples of the backtraced neurons in the VTA at the bregma level -3.08 mm in Sst-Cre mouse. The image on the right shows retrobeads in the injection site (VP). The yellow circle shows the actual unilateral injection spot. On the top left, the green rectangle shows ipsilaterally traced neurons. The lower panel is the magnified image of the green rectangle. *ac* – anterior commissure; *cc* – corpus callosum; *CPu*- caudatus-putamen (striatum); *PBP* – parabrachial pigmented nucleus of the VTA; *VP* – ventral pallidum; *VTA* – ventral tegmental area.

bioRxiv preprint doi: https://doi.org/10.1101/2023.01.06.522982; this version posted January 6, 2023. The copyright holder for this preprint (which was not certified by peer review) is the author/funder, who has granted bioRxiv a license to display the preprint in perpetuity. It is made available under aCC-BY-ND 4.0 International license.

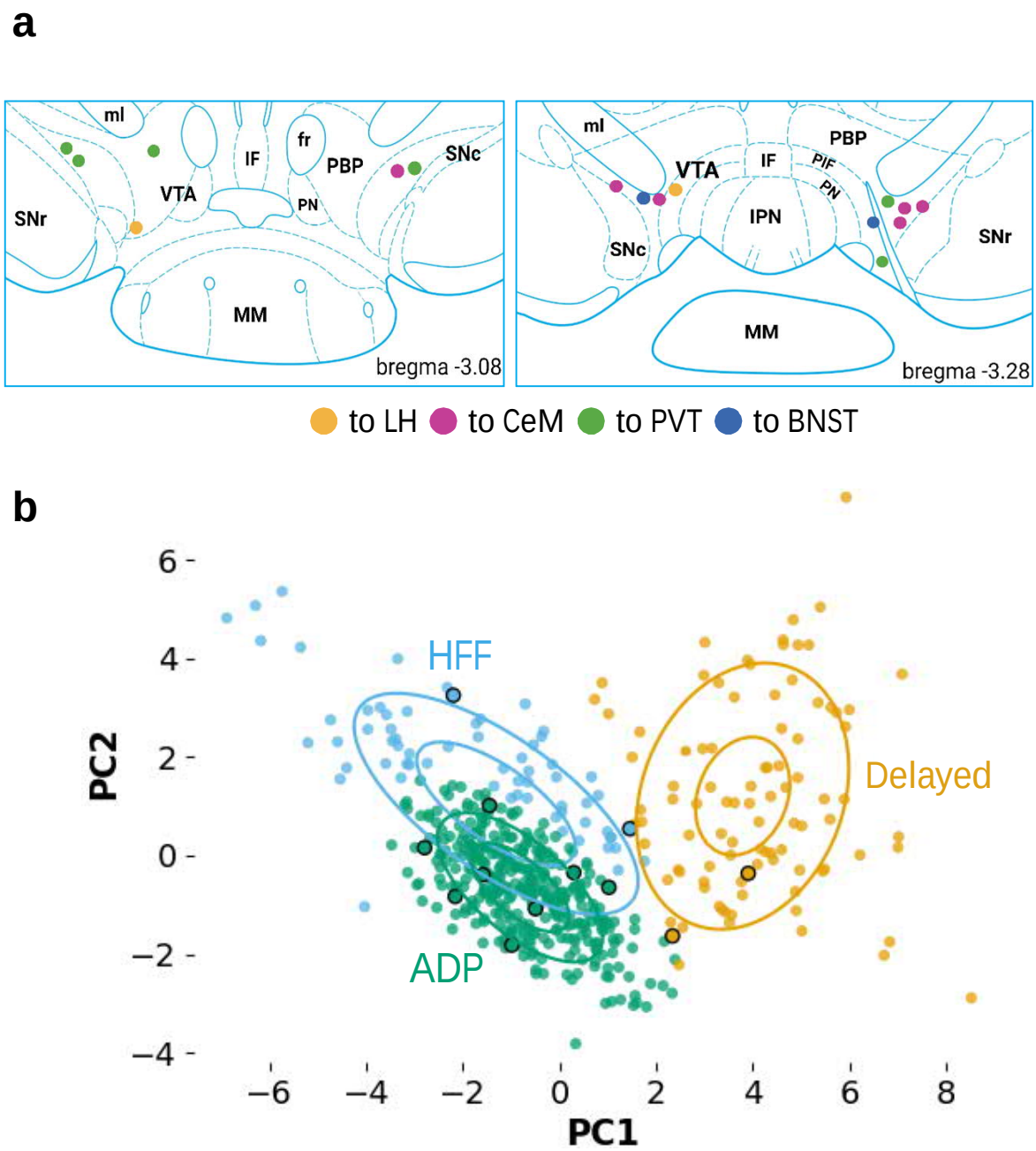

Figure S5. Location of the electrophysiologically recorded VTA Sst neurons projecting to forebrain regions and their electrophysiological subtypes. a. None of the backtraced neurons in electrophysiological experiments were found more posterior than the bregma level -3.28 mm, and most of them were located in the lateral nuclei of the VTA. Their projection sites are colour-coded. b. Most of the recorded backtraced VTA neurons (black-circled) were assigned to the ADP cluster by unsupervised clustering procedure with a previously published dataset of the VTA Sst neurons as the reference. (The method and clusters were described previously in Nagaeva et el., 2020 – see Fig.3). *BNST* – bed nucleus of the stria terminalis; *CeM* – central amygdala, medial part; *LH* – lateral hypothalamus; *PVT* – paraventricular nucleus of the thalamus. ADP – afterdepolarizing, HFF – high-frequency firing.

bioRxiv preprint doi: https://doi.org/10.1101/2023.01.06.522982; this version posted January 6, 2023. The copyright holder for this preprint (which was not certified by peer review) is the author/funder, who has granted bioRxiv a license to display the preprint in perpetuity. It is made available under aCC-BY-ND 4.0 International license.

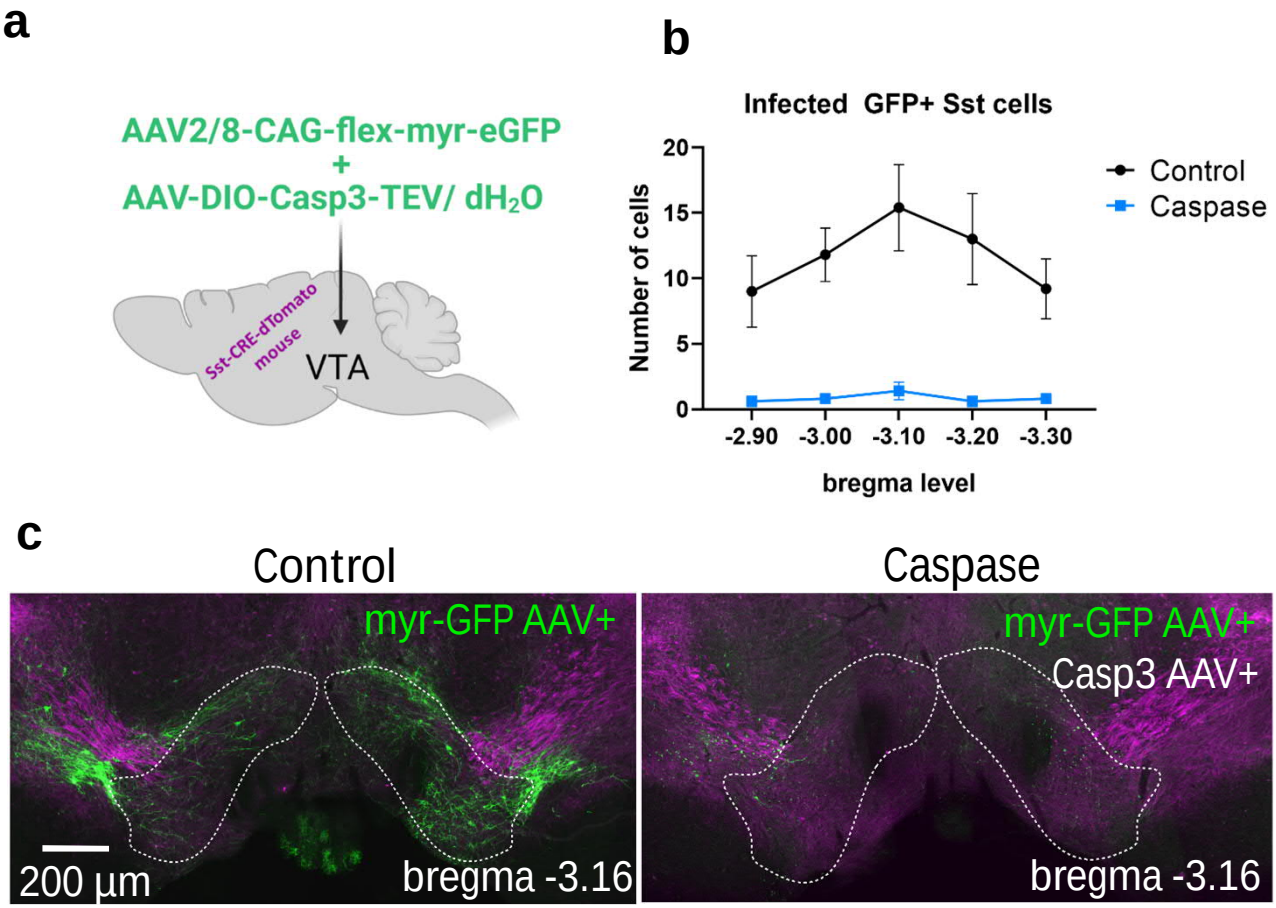

Figure S6. Deletion of the VTA Sst neurons with caspase 3 expressing virus. a. Scheme of the bilateral intra-VTA viral injections to Sst-tdTomato (magenta) mice. The control group received only myr-eGFP virus diluted with dH_20 to adjust the final volume. b. The graph shows an average number of GFP+ Sst cell bodies in the control and caspase-treated animals (n=5 animals per group) depicted per bregma level (X-axis). c. Example images of the mouse coronal VTA section from the control (on the left) and caspase group (on the right). The caspase image has almost no infected GFP+ cell bodies in the VTA region (outlined with a white dashed line), showing only sparse GFP+ neurite fragments of the dead Sst neurons.

bioRxiv preprint doi: https://doi.org/10.1101/2023.01.06.522982; this version posted January 6, 2023. The copyright holder for this preprint (which was not certified by peer review) is the author/funder, who has granted bioRxiv a license to display the preprint in perpetuity. It is made available under aCC-BY-ND 4.0 International license.

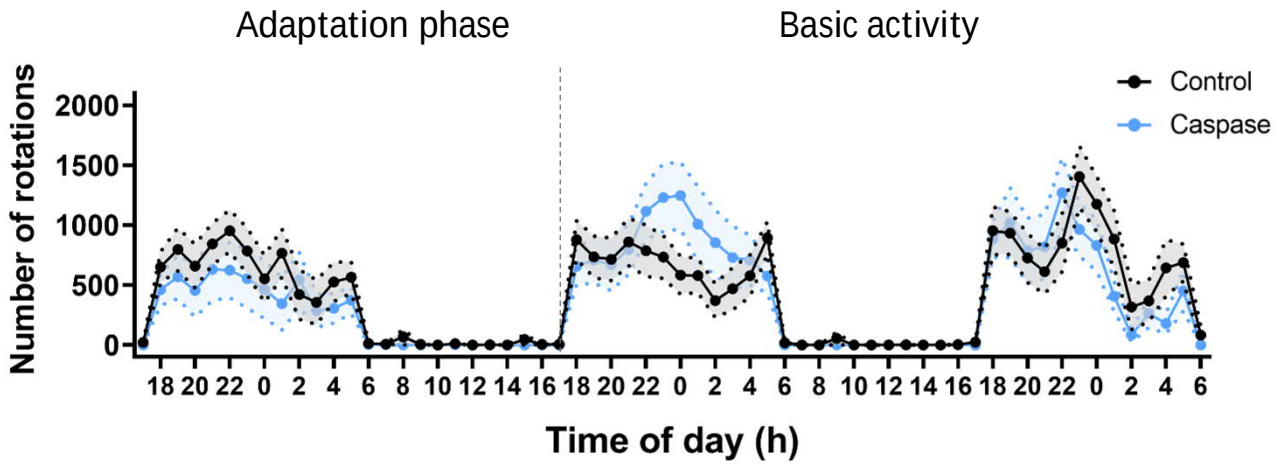

Figure S7. Deletion of VTA Sst neurons did not affect circadian activity in the free-running wheel test (lights on 6-18). Activity of the control (black) and VTA^{Sst}-caspase (blue) mice. There were no differences in the number of rotations between the treatment groups across three days (treatment: $F(1,24)=0.202$, $p=0.657$; treatment x time: $F(67,1608)=1.230$, $p=0.278$). Data are shown as means ± SEM.

bioRxiv preprint doi: https://doi.org/10.1101/2023.01.06.522982; this version posted January 6, 2023. The copyright holder for this preprint (which was not certified by peer review) is the author/funder, who has granted bioRxiv a license to display the preprint in perpetuity. It is made available under aCC-BY-ND 4.0 International license.

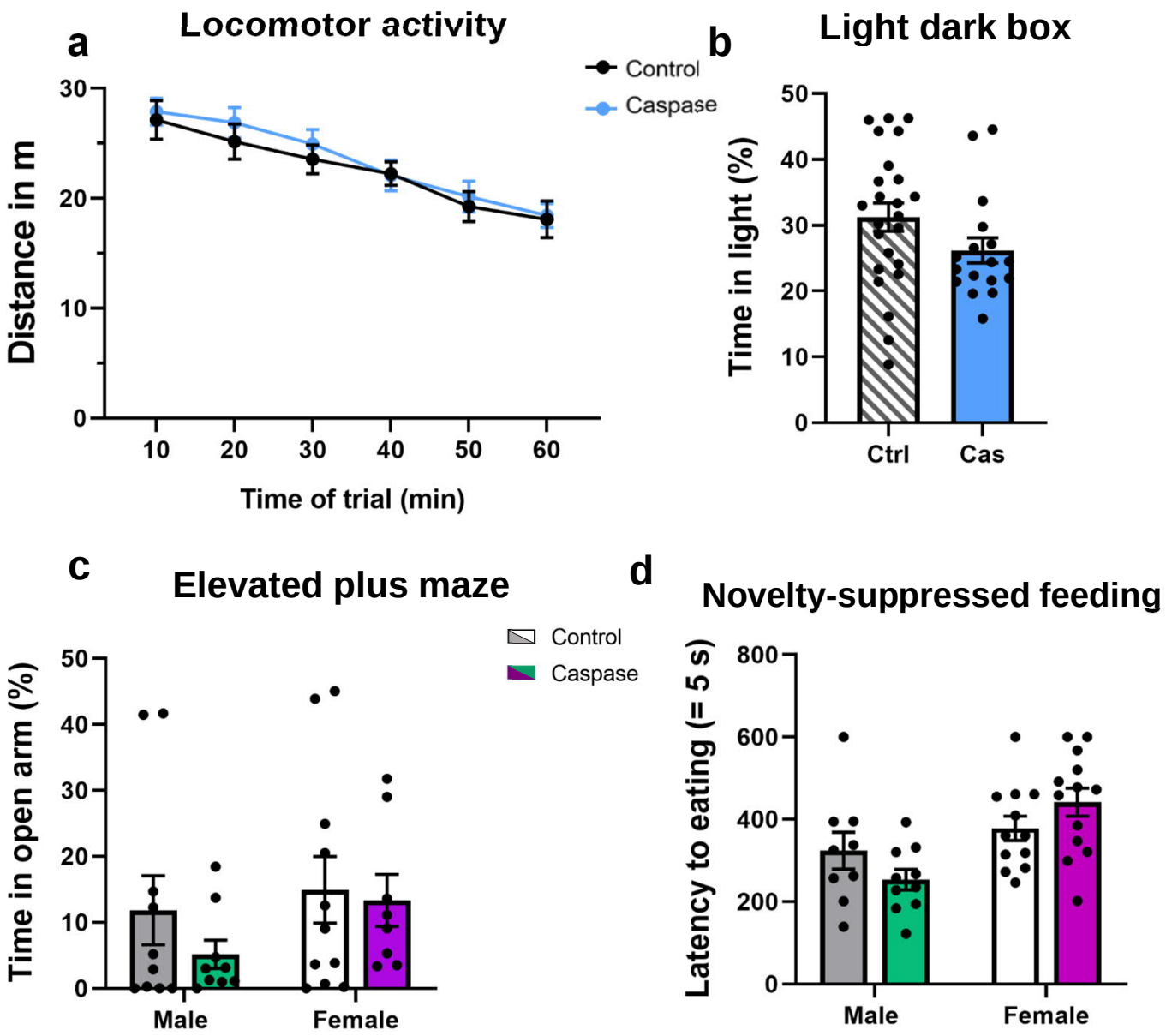

Figure S8. Deletion of Sst neurons in the VTA had no effect on locomotor activity or anxiety-like behaviour. a. Locomotor activity in the open arena was not different between the VTA^{Sst}-caspase and control mice ($F(1,34) = 0.265$, $p = 0.61$). b. The light-dark box test did not show any difference in percentage of time spent in the light compartment between the treatment groups ($F(1,34) = 1.750$, $p=0.195$, sex $F(1,34) = 3.957$, $p= 0.055$). c. Similarly, percentage of time spent in the open arm measured in the elevated plus maze test was not different. d. Latency to start eating in a novel environment did not show a difference, albeit a marginal significance for sex-dependent effects was detected in the VTA^{Sst}-caspase mice (treatment x sex: $F(1,34) = 3.862$, $p = 0.058$). Data are shown as mean ± SEM.

bioRxiv preprint doi: https://doi.org/10.1101/2023.01.06.522982; this version posted January 6, 2023. The copyright holder for this preprint (which was not certified by peer review) is the author/funder, who has granted bioRxiv a license to display the preprint in perpetuity. It is made available under aCC-BY-ND 4.0 International license.

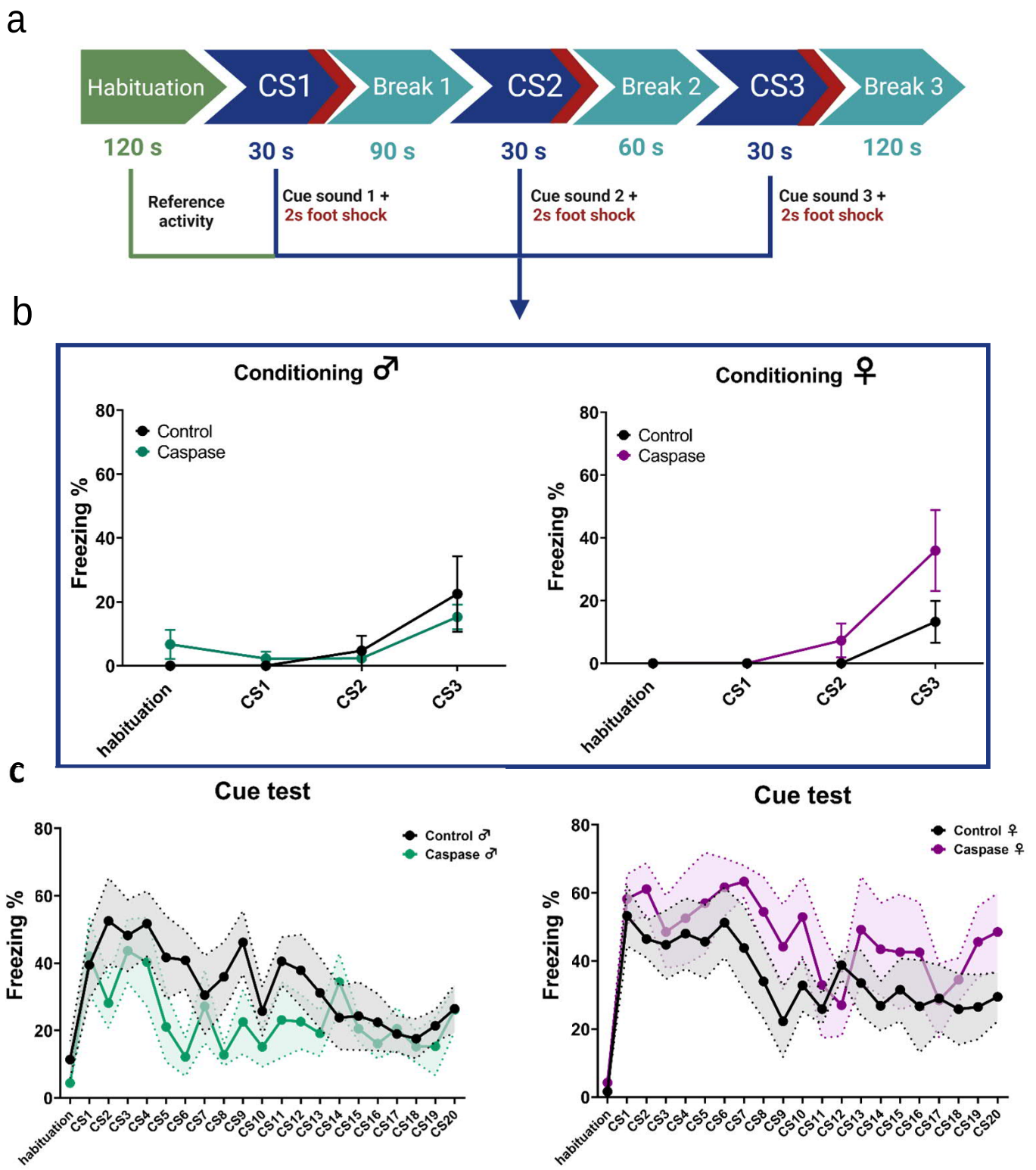

Figure S9. Deletion of the VTA Sst neurons did not affect cue-induced fear processing in Pavlovian fear conditioning. a. Protocol of fear conditioning during the acquisition phase. b. Graphs show per cent freezing (freeze time/total time) during 30-s cue-sound presentations, co-terminated with 2-s foot shocks. There was no difference in freezing between sexes ($F(1,19)=0.019$, $p=0.891$) or between treatments ($F(1,19)=2.182$, $p=0.156$) . c. Similarly, there were no significant difference in rates of cue-associated fear memory retrieval or extinction (cue x sex x treatment: $F(1,420)=1.04$, $p=0.413$).

bioRxiv preprint doi: https://doi.org/10.1101/2023.01.06.522982; this version posted January 6, 2023. The copyright holder for this preprint (which was not certified by peer review) is the author/funder, who has granted bioRxiv a license to display the preprint in perpetuity. It is made available under aCC-BY-ND 4.0 International license.

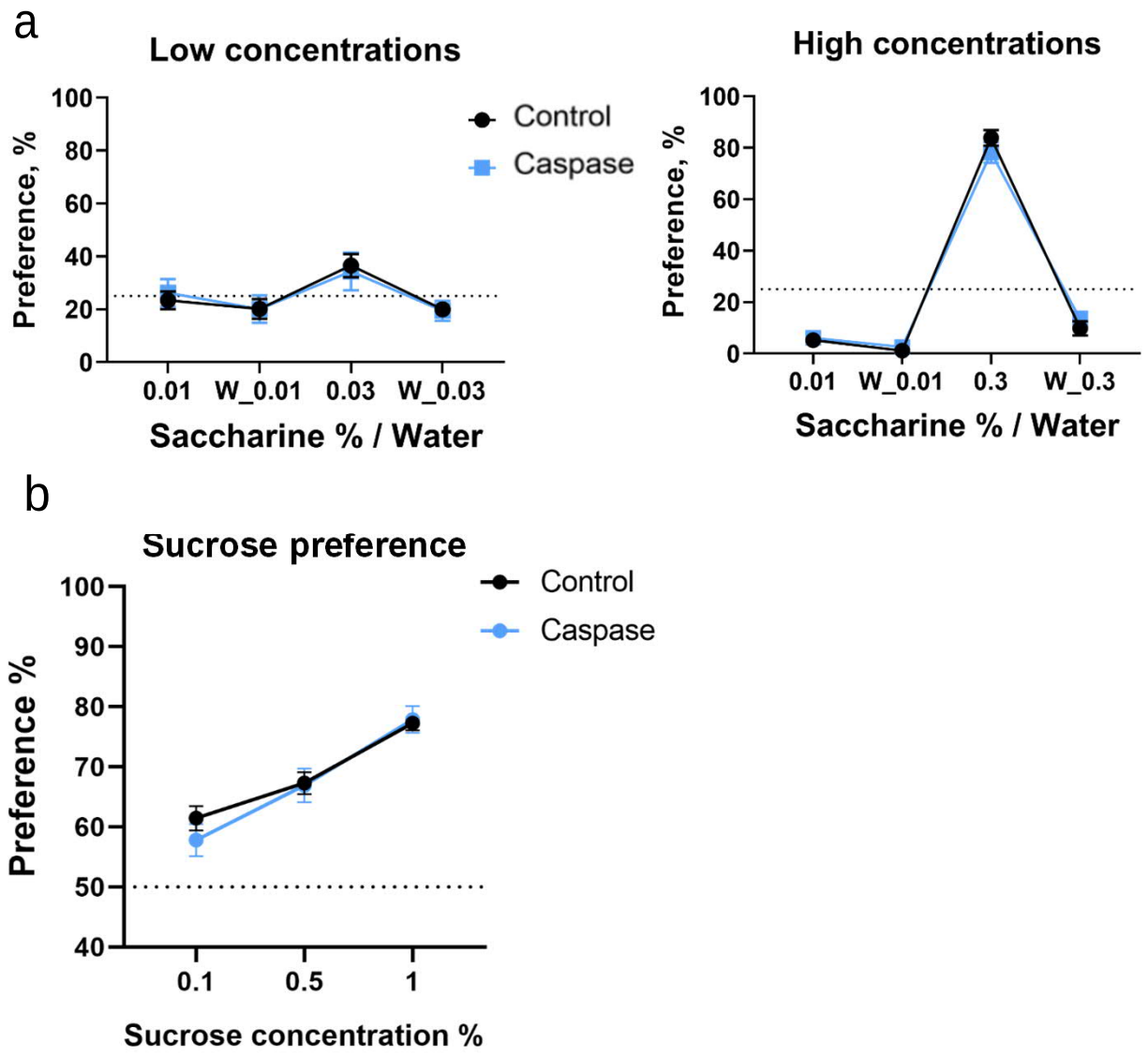

Figure S10. Deletion of the VTA Sst neurons did not affect natural reward preference or sensitivity. Graphs show preference in % (number of licks to a certain bottle/number of total licks, Y-axis) to different saccharine concentrations over water (X-axis). a. Preference to different saccharine concentrations or water in the corresponding corner in the Intellicage system did not reveal any significant differences between the treatment groups for low saccharine concentrations ($F(1,24)=0.698$, $p=0.413$) or to high ones ($F(1,24)=0.045$, $p=0.834$). The dashed line shows a 25% preference rate. b. Similarly, sucrose preference in the two-bottle choice test in individual cages did not reveal any differences (concentration x treatment: $F(2,66) = 0.362$, $p = 0.688$). The dashed line shows a 50% preference rate. Data are shown as mean ± SEM.

bioRxiv preprint doi: https://doi.org/10.1101/2023.01.06.522982; this version posted January 6, 2023. The copyright holder for this preprint (which was not certified by peer review) is the author/funder, who has granted bioRxiv a license to display the preprint in perpetuity. It is made available under aCC-BY-ND 4.0 International license.

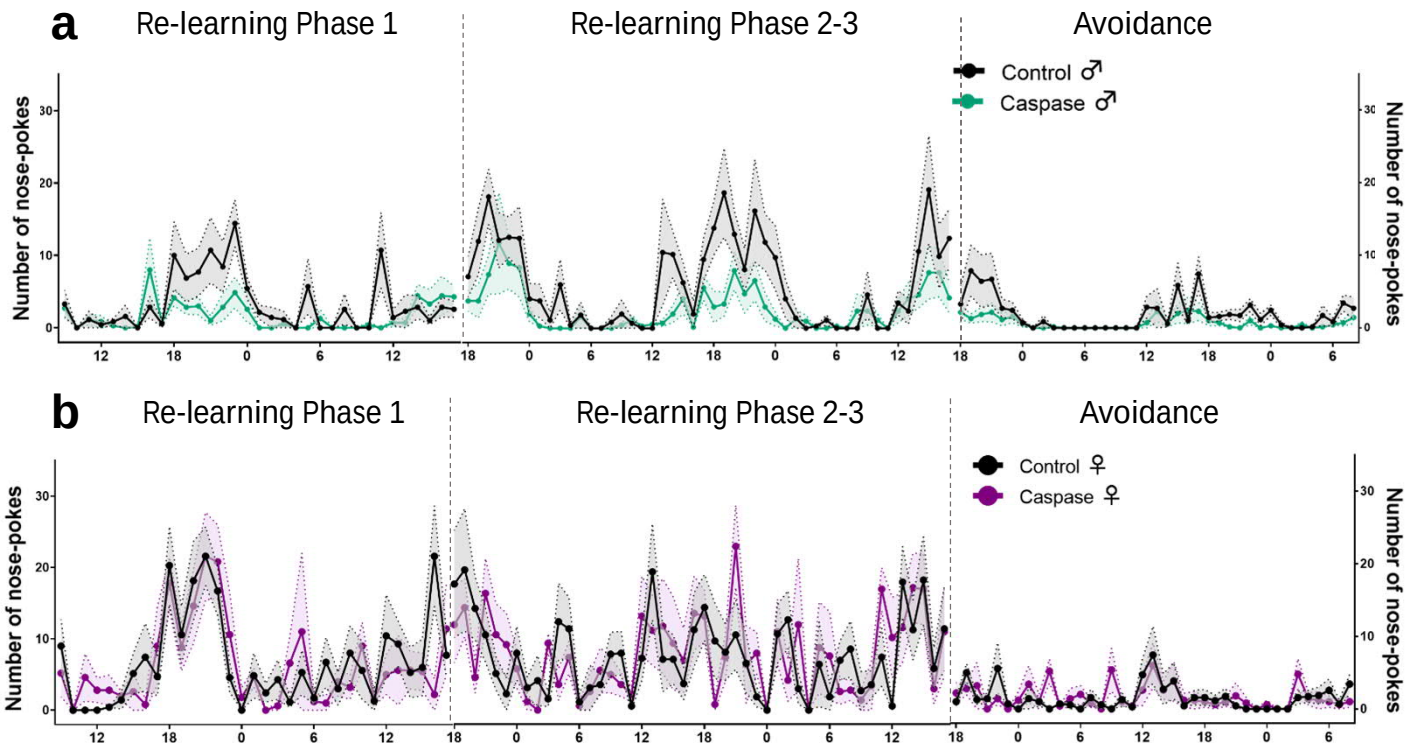

Figure S11. Re-learning new rules in control and caspase mice and introduction of air-puffs in the reward-related task. The X-axis shows the number of nose-pokes to the saccharine bottles per hour, Y-axis shows daily hours (lights on 6-18). a. Nose-poking dynamics in male mice. Although there was a clear tendency in VTA^{Sst}-caspase male mice to be less active in nose-poking to the saccharine corner in all phases of the re-learning-avoidance test, no statistically significant differences were detected between the groups (see Table S1). b. Nose-poking dynamics in female mice showed no differences between the groups.

bioRxiv preprint doi: https://doi.org/10.1101/2023.01.06.522982; this version posted January 6, 2023. The copyright holder for this preprint (which was not certified by peer review) is the author/funder, who has granted bioRxiv a license to display the preprint in perpetuity. It is made available under aCC-BY-ND 4.0 International license.

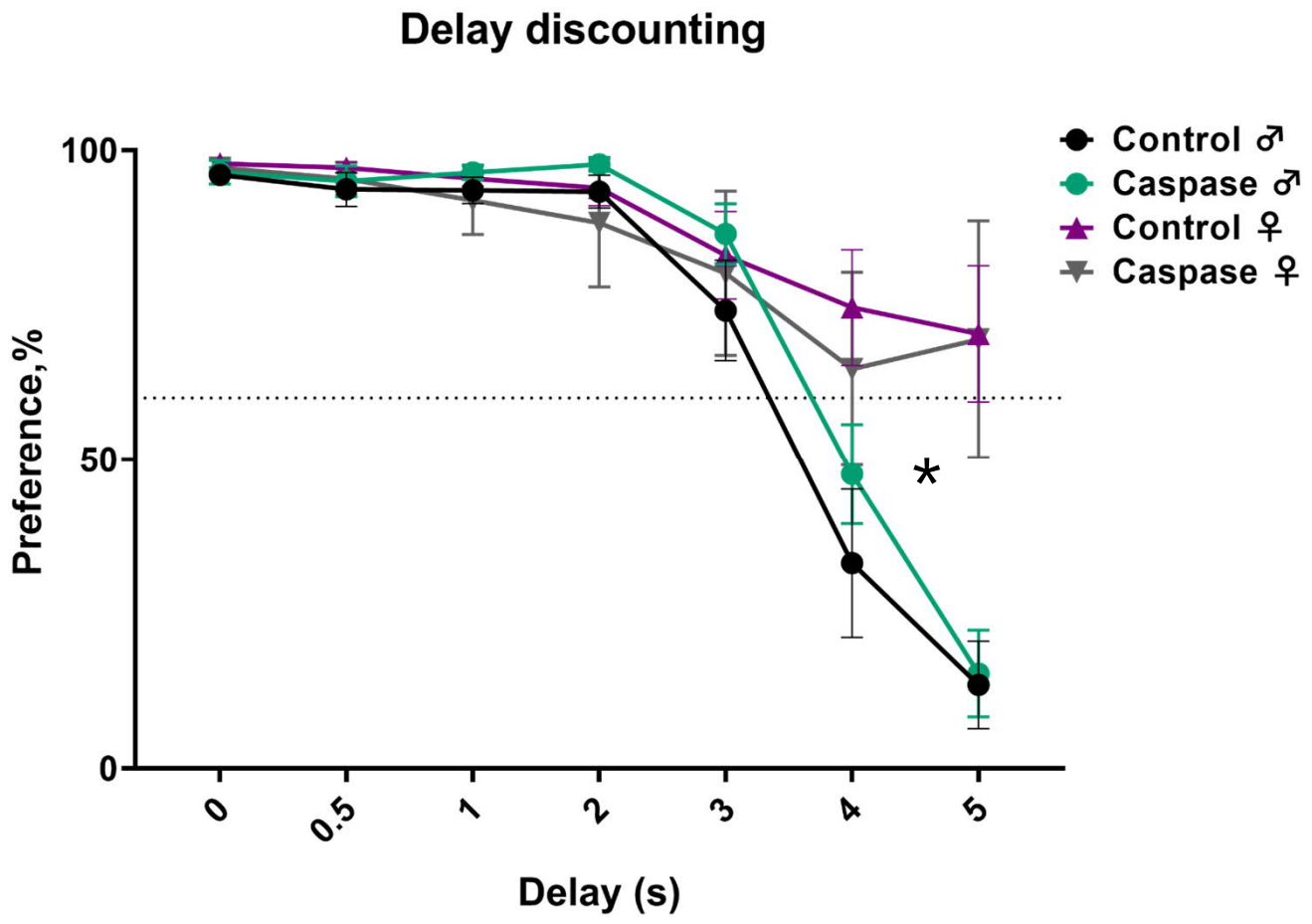

Figure S12. Deletion of the VTA Sst neurons did not influence the impulsivity or readiness to wait for the saccharine reward. Y-axis indicates preference in % for 0.3% saccharine over water defined as a lick number to the saccharine bottle/total number of licks. The X-axis indicates the duration of the delay before the saccharine door opened after a mouse entered the corner. * indicates the significance of the differences between the sexes ($F(1,22)=5.829$, $p=0.024$) and of the sex x delay interaction ($F(6,132)=17.09$, $p<0.0001$).

bioRxiv preprint doi: https://doi.org/10.1101/2023.01.06.522982; this version posted January 6, 2023. The copyright holder for this preprint (which was not certified by peer review) is the author/funder, who has granted bioRxiv a license to display the preprint in perpetuity. It is made available under aCC-BY-ND 4.0 International license.

Intellicage

Supplementary Table 1

Home cage activity

RM - repeated measures

Number of nose-pokes									
Adaptation (14 hours)	RM-2 way ANOVA	F	p value		post-hoc				
	Sex	F(1,22)=24.45	<0.001	****	males		females		
	Treatment	F(1,22)=4.543	0.044	*	0.698	ns	0.004	***	
	Sex*Treatment	F(1,22)=7.085	0.014	*					
Day 2 (24 hours)	RM-2 way ANOVA	F	p value		post-hoc				
	Sex	F(1,22)=5.751	0.025	*	males		females		
	Treatment	F(1,22)=2.770	0.11	ns	0.647	ns	0.03	**	
	Sex*Treatment	F(1,22)=3.133	0.091	ns					
Day 3 (24 hours)	RM-2 way ANOVA	F	p value		post-hoc				
	Sex	F(1,22)=18.315	<0.001	****	males		females		
	Treatment	F(1,22)=4.884	0.038	*	0.647	ns	0.002	**	
	Sex*Treatment	F(1,22)=8.043	0.01	*					
All 3 days (62 hours)	RM-2 way ANOVA	F	p value		post-hoc				
	Sex	F(1,22)=27.329	<0.001	****	males		females		
	Treatment	F(1,22)=7.409	0.012	*	0.695	ns	<0.001	****	
	Sex*Treatment	F(1,22)=10.618	0.004	**					
Number of corner visits									
Adaptation (14 hours)	RM-2 way ANOVA	F	p value		post-hoc				
	Sex	F(1,22)=4.53	0.045	*	males		females		
	Treatment	F(1,22)=2.131	0.158	ns	0.892	ns	0.047	*	
	Sex*Treatment	F(1,22)=2.707	0.114	ns					
Day 2 (24 hours)	RM-2 way ANOVA	F	p value		post-hoc				
	Sex	F(1,22)=0.013	0.909	ns	males		females		
	Treatment	F(1,22)=0.069	0.795	ns	0.388	ns	0.258	ns	
	Sex*Treatment	F(1,22)=2.104	0.161	ns					
Day 3 (24 hours)	RM-2 way ANOVA	F	p value		post-hoc				
	Sex	F(1,22)=13.796	0.001	***	males		females		
	Treatment	F(1,22)=1.443	0.242	ns	0.798	ns	0.076	ns	
	Sex*Treatment	F(1,22)=2.406	0.135	ns					
All 3 days (62 hours)	RM-2 way ANOVA	F	p value		post-hoc				
	Sex	F(1,22)=5.758	0.025	*	males		females		
	Treatment	F(1,22)=0.182	0.182	ns	0.574	ns	0.026	*	
	Sex*Treatment	F(1,22)=4.62	0.043	*					
Number of licks									
Adaptation (14 hours)	RM-2 way ANOVA	F	p value		post-hoc				
	Sex	F(1,22)=22.97	<0.001	****	males		females		
	Treatment	F(1,22)=0.633	0.435	ns	0.605	ns	0.556	ns	
	Sex*Treatment	F(1,22)=0.008	0.931	ns					
Day 2 (24 hours)	RM-2 way ANOVA	F	p value		post-hoc				
	Sex	F(1,22)=0.001	0.97	ns	males		females		
	Treatment	F(1,22)=0.709	0.409	ns	0.388	ns	0.258	ns	
	Sex*Treatment	F(1,22)=0.272	0.608	ns					
Day 3 (24 hours)	RM-2 way ANOVA	F	p value		post-hoc				
	Sex	F(1,22)=1.716	0.204	ns	males		females		
	Treatment	F(1,22)=1.802	0.193	ns	0.578	ns	0.206	ns	
	Sex*Treatment	F(1,22)=0.339	0.567	ns					
All 3 days (62 hours)	RM-2 way ANOVA	F	p value		post-hoc				
	Sex	F(1,22)=2.046	0.167	ns	males		females		
	Treatment	F(1,22)=1.390	0.251	ns	0.647	ns	0.253	ns	
	Sex*Treatment	F(1,22)=0.307	0.585	ns					

Conclusion: caspase animals overall nose poke more, but do not drink more (number of licks)
only caspase females significantly nosepoke and visit corners more than control females
no signinfican difference in males between the treatment groups

bioRxiv preprint doi: https://doi.org/10.1101/2023.01.06.522982; this version posted January 6, 2023. The copyright holder for this preprint (which was not certified by peer review) is the author/funder, who has granted bioRxiv a license to display the preprint in perpetuity. It is made available under aCC-BY-ND 4.0 International license.

Supplementary Table 1

Delay discounting

Number of licks to saccharine bottle	RM-2 way ANOVA	F	p value	
	Sex	F(1,22)=5.889	0.0239	*
	Treatment	F(1,22)=0.032	0.859	ns
	Sex*Treatment	F(1,22)=0.836	0.37	ns
	Sex*Delay	F(6,132)=17.09	<0.001	****

Conclusion: no significant difference between Treatment groups of both sexes
males are ready to wait saccharine less time than females

Saccharine learning and unlearning (number of nose pokes)

Adaptation	RM-2 way ANOVA	F						
	Sex	F(1,22)=23.854	<0.001	****				
	Treatment	F(1,22)=1.217	0.282	ns				
	Sex*Treatment	F(1,22)=0.417	0.525	ns				
Basic activity	RM-2 way ANOVA	F						
	Sex	F(1,22)=53.712	<0.001	****				
	Treatment	F(1,22)=1.345	0.259	ns				
	Sex*Treatment	F(1,22)=2.094	0.162	ns				
Unlearning	RM-2 way ANOVA	F			post-hoc			
"prediction error"	Sex	F(1,22)=33.575	<0.001	****	males		females	
	Treatment	F(1,22)=0.522	0.478	ns	0.3	ns	0.064	ns
	Sex*Treatment	F(1,22)=4.635	0.043	*				

Conclusion: females are more active than males in both treatment groups
Caspase females have a tendency to unlearn slower than the control female group but it is not significant

Saccharine re-learning and avoidance (number of nose pokes)

Adapatation	RM-2 way ANOVA	F			post-hoc			
("re-learning")	Sex	F(1,22)=11.964	<0.001	****	males		females	
	Treatment	F(1,22)=1.547	0.227	ns	0.193	ns	0.659	ns
	Sex*Treatment	F(1,22)=0.323	0.576	ns				
Basic activity	RM-2 way ANOVA	F			post-hoc			
	Sex	F(1,22)=8.298	0.009	**	males		females	
	Treatment	F(1,22)=2.082	0.163	ns	0.034	*	0.917	ns
	Sex*Treatment	F(1,22)=2.557	0.124	ns				
Avoidance	RM-2 way ANOVA	F			post-hoc			
"air-puffs" introduced	Sex	F(1,22)=0.617	0.441	ns	males		females	
	Treatment	F(1,22)=1.939	0.178	ns	0.03	*	0.816	ns
	Sex*Treatment	F(1,22)=3.026	0.096	ns				
Full dynamics	RM-2 way ANOVA	F			post-hoc			
	Sex	F(1,22)=11.964	0.002	**	males		females	
	Treatment	F(1,22)=2.069	0.164	ns	0.047	*	0.982	ns
	Sex*Treatment	F(1,22)=1.975	0.174	ns				

Conclusion: females are more active than males in both treatment groups, but not after the air-puffs were introduced
No differences in the re-learning or avoidance rates between treatment groups.

bioRxiv preprint doi: https://doi.org/10.1101/2023.01.06.522982; this version posted January 6, 2023. The copyright holder for this preprint (which was not certified by peer review) is the author/funder, who has granted bioRxiv a license to display the preprint in perpetuity. It is made available under aCC-BY-ND 4.0 International license.

FEAR CONDITIONING

Supplementary Table 2

FEAR ACQUISITION (conditioning)

pcnt freezing (PF)	RM-2 way ANOVA	F	p value		post-hoc		post-hoc
	Sex	F(1,19)=0.14	0.906	ns	males		females
	Treatment	F(1,19)=0.499	0.488	ns	0.071	ns	0.017 *
	Sex*Treatment	F(1,19)=10.459	0.004	**	tendency that		caspase freeze more
	Point*Sex*Treatment	F(6,114)=4.046	0.012	*	caspase freeze less		
freezing episodes (FE)	RM-2 way ANOVA	F	p value		RM - repeated measures		
	Sex	F(1,19)=0.951	0.342	ns			
	Treatment	F(1,19)=0.419	0.525	ns	*no within Sexes*		
	Sex*Treatment	F(1,19)=5.159	0.035	*			
PF aqusition only BREAKS	RM-2 way ANOVA	F			post-hoc		post-hoc
pcnt freezing	Sex	F(1,19)=0.028	0.869	ns	males		females
	Treatment	F(1,19)=0.033	0.857	ns	0.036	*	0.038 *
	Sex*Treatment	F(1,19)=9.971	0.005	**	caspase freeze less		caspase freeze more
FE aqusition only BREAKS	RM-2 way ANOVA	F	p value				
	Sex	F(1,19)=1.368	0.257	ns			
	Treatment	F(1,19)=0.120	0.733	ns	*no within Sexes*		
	Sex*Treatment	F(1,19)=4.828	0.041	*			
No difference in only Cue Sounds (CS) periods							
	RM-2 way ANOVA	F	p value				
pcnt freezing	Sex	F(1,19)=0.019	0.891	ns			
	Treatment	F(1,19)=2.182	0.156	ns			
	Sex*Treatment	F(1,19)=2.390	0.139	ns			

CONTEXT RETRIEVAL 9 DAYS AFTER

pcnt freezing (PF)	2 way ANOVA	F	p value		post-hoc		post-hoc
	Sex	F(1,21)=1.191	0.288	ns	males		females
	Treatment	F(1,21)=0.18	0.894	ns	0.08	ns	0.086 ns
	Sex*Treatment	F(1,21)=6.602	0.018	*			
Freezing episodes (FE)	2 way ANOVA	F	p value		post-hoc		post-hoc
	Sex	F(1,21)=0.25	0.876	ns	males		females
	Treatment	F(1,21)=3.269	0.085	ns	0.622	ns	0.01 *
	Sex*Treatment	F(1,21)=6.102	0.022	*			caspase freeze more often

CUE-INDUCED RETRIVAL AND EXTINCTION

	RM-2 way ANOVA	F	p value	
	Sex	F(1,21)=4.156	0.54	ns
	Treatment	F(1,21)=0.322	0.577	ns
	Sex*Treatment	F(1,21)=1.823	0.191	ns
	Cue*Treatment	F(20,420)=0.78	0.642	ns
	Cue*Sex*Treatment	F(20,420)=1.040	0.41	ns
no difference in CS retrieval				

bioRxiv preprint doi: https://doi.org/10.1101/2023.01.06.522982; this version posted January 6, 2023. The copyright holder for this preprint (which was not certified by peer review) is the author/funder, who has granted bioRxiv a license to display the preprint in perpetuity. It is made available under aCC-BY-ND 4.0 International license.

OTHER BEHAVIOURAL TESTS

Supplementary Table 3

NOVELTY-INDUCED LOCOMOTION (60 min)				
Distanced moved	RM-2 way ANOVA	F	p-value	
10 min bins	Treatment	F(1,34) = 0.265	0.61	ns
	Treatment*sex	F(1,34) = 0.203	0.655	ns
	Treatment*time	F(5,170) =0.43	0.782	ns
No difference				

RM - repeated measures

LIGHT-DARK BOX TEST				
Time spent in light (%)	2 way ANOVA	F	p-value	
	Sex	F(1,34) = 3.957	0.055	ns
	Treatment	F(1,34) = 1.75	0.195	ns
	Treatment*sex	F(1,34) = 0.704	0.407	ns
No difference				

ELEVATED PLUS MAZE				
Time spent in open arm (%)	RM-2 way ANOVA	F	p-value	
	Sex	F(1,34) = 2.656	0.112	ns
	Treatment	F(1,34) = 0.072	0.79	ns
	Treatment*sex	F(1,34) = 0.394	0.534	ns
No difference				

RUNNING WHEEL (RW) ACTIVITY				
3 Days activity	RM-2 way ANOVA	F	p-value	
	Sex	F(1,24) = 1.470	0.237	ns
	Treatment	F(1,24) = 0.202	0.657	ns
	Treatment*sex	F(1,24) = 1.574	0.222	ns
	Treatment*time	F(67,1608) = 1.230	0.278	ns
	Treatment*time*sex	F(67,1608) = 0.729	0.683	ns
No difference				

NOVELTY-SUPPRESSED FEEDING				
Latency to eating	2 way ANOVA	F	p-value	
	Sex	F(1,34) = 0.543	0.47	ns
	Treatment	F(1,34) = 0.029	0.865	ns
	Treatment * sex	F(1,34) = 3.862	0.058	ns
No difference				

FORCED SWIM TEST				
Latency to immobilization	2 way ANOVA	F	p-value	
	Sex	F(1,34) = 0.33	0.858	ns
	Treatment	F(1,34) = 5.08	0.031	*
	Treatment * sex	F(1,34) = 0.989	0.327	ns
Caspase display longer latency to first immobility				
Duration of immobiliation	RM-2 way ANOVA	F	p-value	
2 min bins	Sex	F(1,34) = 0.611	0.611	ns
	Treatment	F(1,34) = 0.263	0.214	ns
	Treatment * sex	F(1,34) = 0.08	0.778	ns
No difference				

bioRxiv preprint doi: https://doi.org/10.1101/2023.01.06.522982; this version posted January 6, 2023. The copyright holder for this preprint (which was not certified by peer review) is the author/funder, who has granted bioRxiv a license to display the preprint in perpetuity. It is made available under aCC-BY-ND 4.0 International license.

Supplementary Table 3

MORPHINE-INDUCED MOTOR SENSITIZATION				
Induction	RM-2 way ANOVA	F	p-value	
Distance moved	Sex	F(1,32) = 0.04	0.95	ns
10 min bins	Treatment	F(1,32) = 0.034	0.854	ns
	Treatment * sex	F(1,32) = 0.12	0.731	ns
	Treatment * time	F(23,736) = 0.153	0.917	ns
	Treatment * time * sex	F(23,736) = 0.146	0.922	ns
No difference				
Challenge	RM-2 way ANOVA	F	p-value	
Δ Distance moved Challenge-Induction	Sex	F(1,32) = 3.0	0.93	ns
10 min bins	Treatment	F(1,32) = 12.014	0.002	**
	Treatment * sex	F(1,32) = 0.654	0.425	ns
	Treatment * time	F(23,736) = 1.649	0.024	*
	Treatment * time * sex	F(23,736) = 2.915	0.166	ns
Upregulation of morphine motor sensitization				

SUCROSE PREFERENCE				
Sucrose preference (%)	RM-2 way ANOVA	F	p-value	
	Sex	F(1,33) = 0.413	0.413	ns
	Treatment	F(1,33) = 0.0	0.995	ns
	Treatment * sex	F(1,33) = 2.347	0.135	ns
	Treatment * concentration	F(2,66) = 0.362	0.688	ns
	Treatment * concentration * sex	F(2,66) = 2.317	0.109	ns
No difference				